



**HAL**  
open science

## Transport of moderately sorted gravel at low bed shear stresses: The role of fine sediment infiltration

E. Perret, Céline Berni, B. Camenen, A. Herrero, K. El Kadi Abderrezzak

### ► To cite this version:

E. Perret, Céline Berni, B. Camenen, A. Herrero, K. El Kadi Abderrezzak. Transport of moderately sorted gravel at low bed shear stresses: The role of fine sediment infiltration. *Earth Surface Processes and Landforms*, 2018, 43 (7), pp.1416-1430. 10.1002/esp.4322 . hal-02069199

**HAL Id: hal-02069199**

**<https://hal.science/hal-02069199v1>**

Submitted on 15 Mar 2019

**HAL** is a multi-disciplinary open access archive for the deposit and dissemination of scientific research documents, whether they are published or not. The documents may come from teaching and research institutions in France or abroad, or from public or private research centers.

L'archive ouverte pluridisciplinaire **HAL**, est destinée au dépôt et à la diffusion de documents scientifiques de niveau recherche, publiés ou non, émanant des établissements d'enseignement et de recherche français ou étrangers, des laboratoires publics ou privés.

# Transport of moderately sorted gravel at low bed shear stresses: the role of fine sediment infiltration

E. Perret<sup>1\*</sup>, C. Berni<sup>1</sup>, B. Camenen<sup>1</sup>, A. Herrero<sup>1,2</sup>, and K. El Kadi Abderrezzak<sup>3</sup>

<sup>1</sup>Irstea, UR HHLY, centre de Lyon-Villeurbanne, 5 rue de la Doua, CS20244, F-69625 Villeurbanne Cedex, France

<sup>2</sup>Now at Catalan Institute for Water Research, 101 Carrer Emili Grahit, 17003, Girona, Spain

<sup>3</sup>EDF R&D, LNHE / LHSV, 6 Quai Watier, F-78401 Chatou, France

\*Corresponding author, e-mail: [emeline.perret@irstea.fr](mailto:emeline.perret@irstea.fr)

May 24, 2018

---

## Abstract

1  
2 A reliable estimation of sediment transport in gravel-bed streams is im-  
3 portant for various practical engineering and biological studies (e.g., chan-  
4 nel stability design, bed degradation/aggradation, restoration of spawning  
5 habitat). In the present work, we report original laboratory experiments in-  
6 vestigating the transport of gravel particles at low bed shear stresses. The  
7 laboratory tests were conducted under unsteady flow conditions inducing low  
8 bed shear stresses, with detailed monitoring of the bed topography using  
9 a laser scanner. Effects of bed surface arrangements were documented by  
10 testing loose and packed bed configurations. Effects of fine sediments were  
11 examined by testing beds with sand, artificial fine sand or cohesive silt infil-  
12 trated in the gravel matrix. Analysis of the experimental data revealed that  
13 the transport of gravel particles depends upon the bed arrangement, the bed  
14 material properties (e.g., size and shape, consolidation index, permeability)  
15 and the concentration of fine sediments within the surface layer of moving  
16 grains. This concentration is directly related to the distribution of fine par-  
17 ticles within the gravel matrix (i.e., bottom-up infiltration or bridging) and

18 their transport mode (i.e., bedload or suspended load). Compared to loose  
19 beds, the mobility of gravel is reduced for packed beds and for beds clogged  
20 from the bottom up with cohesive fine sediments; in both cases, the bed shear  
21 stress for gravel entrainment increases by about 12 %. On the other hand, the  
22 mobility of gravel increases significantly (bed shear stress for particle motion  
23 decreasing up to 40 %) for beds clogged at the surface by non-cohesive sand  
24 particles.

25 **Keywords:** sediment transport; fine sediment clogging; bed arrangement;  
26 incipient motion; laboratory experiments.

---

## 27 Introduction

28 A mountain river is a dynamic system. Its flow and bed morphology change due  
29 to natural events (e.g., changes in flow conditions and sediment supply) or human  
30 activities, resulting in overbank floods, structure failure and fish stock variability  
31 (Pitlick and Van Steeter, 1998). Mountain rivers are often formed with grain sizes  
32 ranging from clay to pebble (diameters between micrometers and decimeters), which  
33 leads to selective sediment transport, fine-coarse particle interactions, infiltration  
34 and clogging of fine sediments within the gravel substrate. The amount and type of  
35 fine sediment found in coarse substrate can have implications for the bed morphology  
36 dynamics, the health of aquatic biota, surface-groundwater interactions as well as  
37 water quality (Kondolf and Wolman, 1993; Wharton et al., 2017).

38 In gravel-bed streams, partial transport induced by low-flow conditions is more  
39 frequent than full mobility (all grain sizes are mobile, the bed surface completely  
40 disrupted due to high flow conditions). Therefore, the bedload rate can be highly  
41 variable in time and space because the entrainment threshold is only slightly ex-  
42 ceeded (Wilcock and McArdell, 1993). In this context, quantitative estimates of  
43 the threshold conditions for particle motion and of gravel bedload at low shear  
44 stresses are difficult (Buffington and Montgomery, 1997). The use of the Shields di-  
45 agram or bedload formulae based on excess bed shear stress, originally developed for  
46 non-cohesive and well-sorted bed materials, is questionable (Wilcock, 2001; Parker,

47 2008). Most of these formulae do not take into account aspects such as: the Grain  
48 Size Distribution (GSD) of bed material; the specific conditions for incipient motion  
49 of each grain-size fraction (Proffitt and Sutherland, 1983); and the role played by  
50 surface bed structures, specifically grain arrangement and orientation (Voepel et al.,  
51 2017), and by fine sediments mortaring the gravel on bed mobility (Hodge et al.,  
52 2013; Wainwright et al., 2015).

53 For poorly (and moderately) sorted gravel materials, the formation of a surface  
54 armor layer is generally observed under steady flow and no sediment feeding condi-  
55 tions (Church et al., 1998; Guney et al., 2013), which implies a bed surface coarsening  
56 (Hassan and Church, 2000), an increase in grain imbrication (Mao et al., 2011; Qin  
57 et al., 2012), and the formation of grain patterns (e.g. clusters, microforms; Marion  
58 et al., 2003; Curran, 2010). Under unsteady flows, Mao (2012) and Guney et al.  
59 (2013) highlighted significant changes in gravel bed surface organization due to the  
60 antecedent flow history and the initial degree of bed armoring and arrangement.  
61 The arrangement of the bed surface was identified as an important factor affecting  
62 gravel mobility, but its effect was not quantified. The transport of bimodal material  
63 formed with sand and gravel mixture was examined mainly in laboratory conditions  
64 (e.g. Ikeda and Iseya, 1988; Wilcock and Crowe, 2003; Curran and Wilcock, 2005),  
65 with the aim of developing empirical formulae for the computation of bedload. In-  
66 creasing sand content, the bed becomes sand-dominant with gravel particles moving  
67 individually over a surface sand layer (Wilcock et al., 2001). Wilcock and Ken-  
68 worthy (2002) developed a two-fraction model for sand-gravel mixture transport.  
69 Wilcock and Crowe (2003) proposed a surface-based transport model for mixed-size  
70 sediments considering the hiding/exposure effect and the nonlinear effect of sand  
71 content.

72 The process of fine sediment infiltration into immobile clean gravel was investi-  
73 gated, mainly for non-cohesive sediments, experimentally (Einstein, 1968; Beschta  
74 and Jackson., 1979; Schälchli, 1992; Haynes et al., 2009; Gibson et al., 2010; Wren  
75 et al., 2011, among others) and theoretically (Sakthivadivel and Einstein, 1970; Cui

76 et al., 2008; Nuñez Gonzalez, 2016; Herrero and Berni, 2016). To a lesser extent, one  
77 can find a number of field (Frostick et al., 1984; Lisle, 1989; Sear, 1993) and labora-  
78 tory experiments examining the infiltration of cohesive sediments (Krishnappan and  
79 Engel, 2006). Depending on the fine-to-coarse particle diameter ratio (Gibson et al.,  
80 2009), two infiltration mechanisms can occur: 1) deep infiltration of fine sediments  
81 down to an impermeable bottom and progressive filling of the gravel pores from the  
82 bottom upward (a process called Unimpeded Static Percolation (USP)); 2) trapping  
83 of fine grains at the surface pore throats that prevents further fine sediments from  
84 infiltrating into the subsurface, therefore forming a surface clogged layer (i.e. bridge  
85 or seal). To the author's knowledge, no study describing how the clogged gravel  
86 material is mobilized is available. Marquis and Roy (2012) argued that fine sedi-  
87 ment infiltration and dynamics may affect gravel bed dilation (i.e., reorganization of  
88 coarse particles into a looser packing) and contraction (i.e., tighter packing) during  
89 low flood events.

90 The role of cohesive sediments (silt/clay) on inception of gravel motion was  
91 investigated in a few field (Reid et al., 1985; Barzilai et al., 2013) and laboratory  
92 studies (Kothyari and Jain, 2008; Jain and Kothyari, 2009). Cohesive particles  
93 consolidate the gravel bed, leading to an interlocking bed structure that modifies  
94 bedload drastically (Hassan and Church, 2000). Gravel transport decreases with  
95 an increase in clay content (Jain and Kothyari, 2009; Barzilai et al., 2013), but  
96 depends on various parameters (e.g., clay type and percentage, water content in  
97 the cohesive fraction, undrained shear strength, unconfined compressive strength,  
98 plasticity index).

99 The review presented above indicates that a considerable amount of effort has  
100 been involved in the investigation of non-cohesive, non-uniform selective sediment  
101 transport leading to an armor layer. Similarly, studies examining the infiltration of  
102 non-cohesive fines through immobile, well-sorted gravel beds are abundant. How-  
103 ever, the transport of gravel at low bed shear stress (i.e., flows generating a very low  
104 but measurable bedload) along with considering the role of fine sediments and struc-

105 tures of the surface bed material has not been examined yet. This is unfortunate,  
106 because understanding the factors controlling the gravel mobility at low bed shear  
107 stress is required to quantify and model bedload in mountain streams. Indeed, the  
108 largest uncertainty in predictive models is observed for this range of low bed shear  
109 stresses (Camenen and Larson, 2005; Recking et al., 2012). Our research addresses  
110 this gap by quantifying the transport of moderately sorted gravel close to the incip-  
111 ient motion conditions. We report the results from a series of original experiments  
112 conducted in a straight laboratory flume under unsteady flow conditions generat-  
113 ing low bed shear stresses. Two different bed configurations (loose vs packed) were  
114 tested to reflect the role of grain arrangement and orientation on gravel mobility.  
115 The effects of fine sediments were examined by infiltrating different types of fine  
116 sediments in the gravel matrix.

117 This paper is organized as follows: after presenting the experimental set-up  
118 and describing how the infiltrated and packed beds were created in the laboratory,  
119 the results and main observed processes are summarized. Then the main factors  
120 affecting gravel transport at low bed shear stresses are discussed; a methodology for  
121 improving the computation of bedload in gravel beds is also presented. The last  
122 section provides concluding remarks.

## 123 **Materials and methods**

### 124 **Experimental facility**

125 The sediment transport experiments were carried out in an 18 m-long, 1 m-wide  
126 and 0.8 m-deep tilting flume with glass walls (Figure 1). This facility is located  
127 in the Irstea's Hydraulic and Hydromorphology Laboratory (HHLab) in Lyon-  
128 Villeurbanne (France). The flume longitudinal slope was set at 1%. An electromag-  
129 netic flowmeter (Krohne Optiflux) measured the flow discharge ( $Q$ ). A honeycomb  
130 straightener eliminated flow turbulent structures at the entrance. A 1 m-long weir  
131 with adjustable slope and height was placed at the downstream end to control the

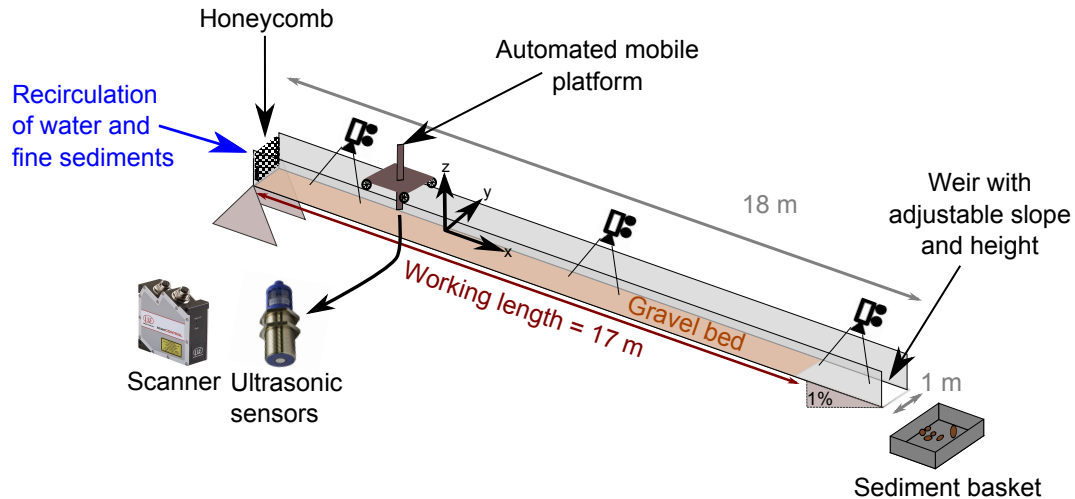


Figure 1: Experimental set-up.

132 water depth and to achieve a uniform flow condition, without impeding bedload.  
133 The flow was qualified as uniform when its free surface was approximately paral-  
134 lel to the longitudinal bed profile. The weir settings were determined after several  
135 trials. In our experiments, the flow depth was the same (within  $\pm 1$  cm) at every  
136 sections of the channel located between 6 and 18 m downstream of the flume inlet.  
137 Ultrasonic sensors (Microsonic mic+130/IU/TC) and a laser scanner (scanControl  
138 2900 Micro-Epsilon, vertical resolution:  $2 \mu\text{m}$ ), installed on an automated mobile  
139 platform, measured the water surface and bed topography, respectively. The analy-  
140 sis of laser scanner surveys provides indicators of bed surface arrangement, such as  
141 the geometrical grain roughness of the bed surface ( $\sigma_{zg}$ ), lengths of the bed surface  
142 structures in the streamwise ( $\Delta_{x0}$ ) and cross-stream direction ( $\Delta_{y0}$ ), the armoring  
143 degree ( $A_r$ ) and the preferential orientation of bed surface grains ( $\Phi$ ) (Marion et al.,  
144 2003; Perret et al., 2016). A closed recirculating system supplied clear water or wa-  
145 ter mixed with fine sediments (grain sizes less than 0.5 mm) into the flume. There  
146 was no upstream gravel feeding. Rolling baskets collected the transported gravel  
147 at the downstream end of the flume, so that bedload rate measurements could be  
148 performed.

149 The experimental configurations were chosen to be representative of alpine rivers  
150 in terms of slope (1%), Shields numbers ( $0.04 \leq \tau^* \leq 0.08$ ), relative roughness (0.08

151  $\leq D/h \leq 0.14$ ) and bed morphology planform (plane or braided beds) (Camenen  
152 et al., 2010).

## 153 Bed material

154 Two types of bed materials were studied: moderately sorted gravel (G) and bimodal  
155 material composed of the same gravel matrix infiltrated with fine sediments (Fig-  
156 ure 2). Three types of fine sediment were used: two were non-cohesive (sand (S)  
157 and artificial fine sand (FS)) and one was cohesive (medium silt (Ms)). Table 1  
158 summarizes the geometrical and geotechnical characteristics of gravel and fine sed-  
159 iments. Hereafter,  $D$  and  $d$  denote diameters of the coarse (G) and fine (S, FS or  
160 Ms) sediments, respectively.

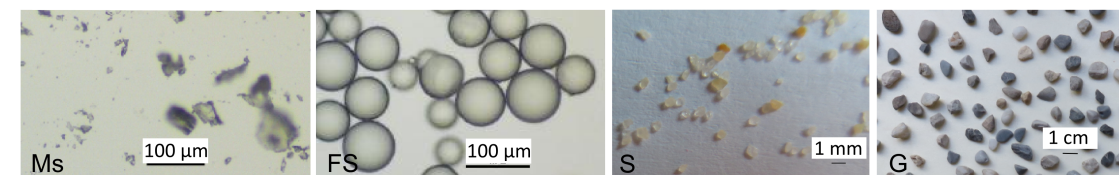
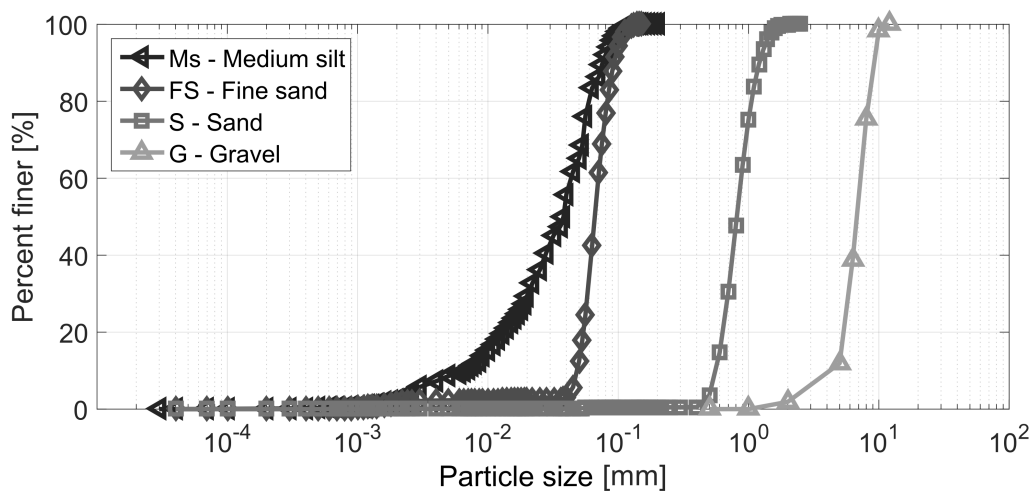


Figure 2: Sediment GSD and shapes. Photographs of Ms and FS were taken with a microscope.

161 Gravel was quite angular with  $D_{50} = 6.8$  mm, where  $D_i$  is the diameter such  
162 that  $i\%$  of grains are finer by weight. Sand was natural and well sorted, with a  
163 median diameter  $d_{50} = 813$   $\mu$ m. Fine Sand (FS) consisted of non-cohesive glass

164 beads with  $d_{50} = 66 \mu\text{m}$ . Medium silt (Ms) was formed of cohesive glass powder,  
165 with  $d_{50} = 40 \mu\text{m}$ , whose size is similar to FS.

166 The circularity index  $C_I$  was chosen as the shape indicator (Table 1). It measures  
167 the 2D grain shape deviation from a perfect circle (changes in grain form, symmetry  
168 or roughness).  $C_I$  was computed using image-post-processing of each sediment shape  
169 (Figure 2,  $C_I = 4\pi A/P^2$ , with  $A$  as the area of the particle projected on the image  
170 and  $P$  the perimeter of the projected area). Around 50 particles of each sediment  
171 material were analysed to obtain statistically relevant indexes.  $C_I = 1$  is associated  
172 with a perfect circle, whereas  $C_I \approx 0$  indicates a distorted shape.

173 Consolidation of fine sediments,  $C_u$ , was determined using a penetrometer (French  
174 norms, XP CEN ISO/TS 17892-6, 2006) and a scissometer (French norms, NF P  
175 94-072, 1995). In the penetrometer test,  $C_u$  corresponds to a dynamic penetration  
176 resistance, whereas in the scissometer test,  $C_u$  is the sediment resistance to a rota-  
177 tional moment.  $C_u$  reported in Table 1 are averaged values given by these two tests.  
178 Tests were performed on water-saturated ( $C_{u\text{-sat}}$ ) and low water content ( $C_{u\text{-20-30\%}}$ )  
179 sediment samples. For Ms,  $C_u$  reaches values similar to those characterizing soft  
180 rocks ( $\geq 250 \text{ kPa}$ ) when the water content is low.

181 Figure 3 illustrates the gravel beds tested. Beds are identified and named ac-  
182 cording to the following nomenclature: *bed arrangement of the gravel matrix* (L  
183 for loose, H for hybrid and P for packed) and *sediments forming the bed material*  
184 (G for gravel, S for sand, FS for fine sand and Ms for medium silt). The following  
185 sections describe how these beds were prepared.

## 186 **Experimental procedure for clean gravel beds**

187 **Preparation of clean gravel beds** - Both loose and packed (L-G and L-P) clean  
188 gravel beds were studied. L-G beds denote loose, random and non-organized gravel  
189 beds that were not subjected to antecedent flows. To create L-G beds, gravel was  
190 manually installed in the flume using a large scraper to obtain an 8 cm-thick flat  
191 bed surface, parallel to the flume bottom. In contrast, antecedent long flows over a

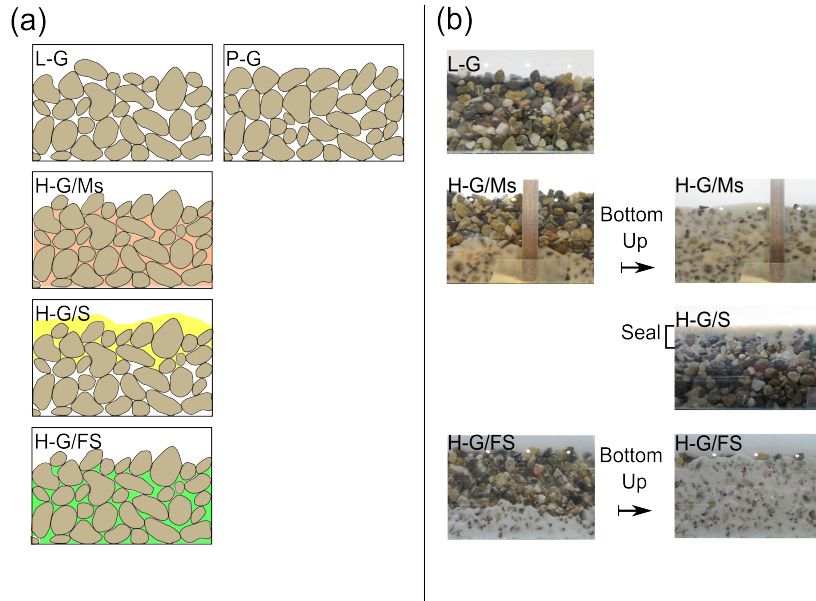


Figure 3: (a) Diagrams illustrating the beds studied and (b) lateral photographs of the beds during (left) and at the end (right) of the infiltration phase.

192 gravel bed were necessary to create a packed and structured bed (P-G bed). The  
 193 P-G bed preparation followed three steps (Figure 4a). In step (1), a L-G bed was  
 194 prepared. In step (2), this bed was subjected to a typical flood hydrograph with  
 195 increasing and decreasing steps of 5 L/s. At the end of step (2), a hybrid bed (H-G)  
 196 was obtained, defined as a bed that had just experienced a flood for a short time.  
 197 The flow discharge  $Q_{\text{ref-F}}$  producing a specified reference transport rate  $q_{s\text{-ref}}$  at the  
 198 falling limb in step (2) was determined.  $q_{s\text{-ref}}$  refers to the first low bedload rate,  
 199 that can be accurately measured considering the large uncertainty linked to bedload  
 200 measurement at low bed shear stresses.  $q_{s\text{-ref}}$  defines the gravel incipient motion  
 201 and should be adapted if a different gravel material was studied (USWES, 1935;  
 202 Parker et al., 1982). In this case,  $Q_{\text{ref-F}}$  corresponds to the discharge for cessation of  
 203 gravel motion on a hybrid bed (i.e. for which gravel transport becomes lower than  
 204  $q_{s\text{-ref}}$ ). This discharge was not exactly the same between two experiments because  
 205 we were not able to reproduce the exact same initial loose bed ( $Q_{\text{ref-F}}$  was within  
 206 the range of 60-65 L.s<sup>-1</sup>). The difficulty to reproduce loose beds was highlighted  
 207 by analysing the laser scanner surveys of their bed surfaces. Laser scanner data  
 208 also show that grain arrangements were present on a H-G bed, although not as

209 pronounced as for a P-G bed. Step (3a) is the arrangement phase. A constant  
 210 discharge of  $Q_{\text{ref-F}}$  was imposed for several hours to enhance a natural bed surface  
 211 arrangement. This arrangement phase was stopped when the gravel transport rate  
 212 became insignificant at the downstream end of the flume, i.e., after approximately  
 213 12 hours. We considered that the P-G bed is created at the end of step (3a).  
 214 Water was then drained out carefully from the flume, keeping the P-G bed surface  
 215 organization intact. Since the P-G bed preparation was carried out with low gravel  
 216 transport, the bed stabilized without significantly changing its longitudinal slope  
 (variation was around 5 % on average).

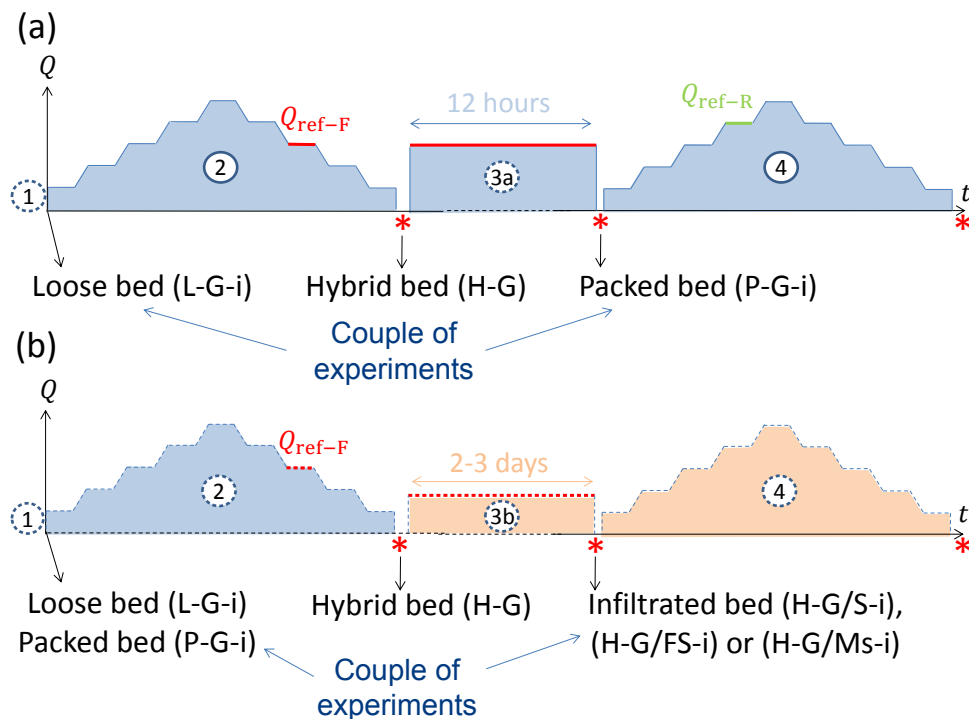


Figure 4: Experimental protocol from bed preparation to bedload experiment for a) clean gravel beds and b) infiltrated gravel beds. Blue areas correspond to clear water flow while orange areas represent fine concentrated water flow. (1) denotes the bed installation, (2) and (4) refer to sediment transport experiments. (3a) and (3b) are bed arrangement phase and infiltration phase, respectively. The symbol \* indicates a drained bed (which can last a few days).  $Q_{\text{ref-R}}$  and  $Q_{\text{ref-F}}$  are the flow discharges for which the initiation of gravel motion (during the rising limb) and the cessation of gravel motion (during the falling limb) were observed, respectively.

217

218 **Sediment transport experiments on clean gravel beds -** For the sake  
 219 of clarity, each test is denoted with the bed nomenclature completed by a num-  
 220 ber  $i$ . Two experiments sharing the same number refer to one *experiment couple*,

221 corresponding to two tests performed successively with no manual gravel bed re-  
222 installation (steps (2) and (4) in Figure 4). For example, a loose bed experiment  
223 conducted before a bed arrangement phase forms a couple with the next packed bed  
224 experiment (e.g. L-G-1 followed by P-G-1). Similarly, two experiments conducted  
225 before and after the infiltration phase form a couple (e.g. L-G-5 and H-G/Ms-5).

226 A sediment transport experiment consisted in operating the flume with a stepped  
227 flow hydrograph while collecting transported gravel periodically at the flume's down-  
228 stream end (Figure 4, step (2) for L-G and step (4) for P-G). The selected hydro-  
229 graphs simulate unsteady flow events, characterized by symmetrical rising and falling  
230 limbs with steady and uniform flow intervals lasting 15 - 20 min and flow transitions  
231 lasting 5 min. Stepped plateaus provide steady flows that can more easily be char-  
232 acterized than a true unsteady flow. In addition, the characteristic time for bed  
233 arrangement was found to be much longer (several hours) (Church et al., 1998) than  
234 the plateau duration. Consequently, we expected the flow to be unsteady from the  
235 sediment transport point of view. Similar hydrographs (i.e., magnitude, duration  
236 and sequencing) were used for all experiments so that they could be compared (see  
237 supplementary files). Before starting each experiment, the bed surface was pho-  
238 tographed and scanned. The transported gravel was collected every 5 min (three  
239 times per interval) in the rolling sieves at the downstream end of the flume and  
240 was then dried and weighed to deduce bedload temporal variations (per unit width)  
241  $q_s(t)$ . Using recorded videos,  $q_s(t)$  was estimated by visually counting gravel passing  
242 through a given area at different locations (i.e., upstream, middle, and downstream  
243 of the channel). The measured bedload rate at the downstream end of the flume was  
244 roughly the same as the one estimated from visual counting; the observed differences  
245 may be the consequence of local variation and long bedload oscillation since  $q_s$  is  
246 averaged over several minutes (Recking et al., 2012). The level of the water sur-  
247 face was measured during each hydrograph plateau at every meter along the flume  
248 centerline; the averaged water depth  $h$  was then calculated. After each sediment  
249 transport experiment, the bed was drained and a topographic survey was carried

250 out.

## 251 **Experimental procedure for infiltrated beds**

252 **Preparation of infiltrated beds** - Bimodal beds (H-G/Ms, H-G/FS, H-G/S)  
253 were not prepared by homogeneously mixing gravel and fine sediments as commonly  
254 done in previous studies (Wilcock et al., 2001; Curran and Wilcock, 2005). Instead,  
255 bimodal beds were prepared by infiltrating fines into a H-G bed, thereby replicating  
256 natural vertical bed structures (Figure 3). Figure 3b shows a side view of the final  
257 beds at the end of each infiltration operation. Table 1 summarizes the geotechnical  
258 properties of the bed materials tested except for the case of a bed infiltrated with  
259 sand particles. Indeed, no average values were estimated for this case because of the  
260 inhomogeneous vertical distribution of sand through the gravel matrix.

261 Figure 4b illustrates how a bimodal bed was prepared. First, a sediment trans-  
262 port experiment (step (2)) was carried out on a specific initial bed (i.e., L-G or P-G)  
263 to obtain a hybrid bed. The bed is designated as hybrid when produced using a  
264 single hydrograph flowing either over a L-G bed or over a P-G bed. In the bimodal  
265 experiments, only experiment H-G/Ms-6 resulted from an initial P-G bed. Hybrid  
266 beds are more reproducible in the laboratory in terms of bed surface arrangements  
267 than loose beds, which is why the infiltration phase (step (3b)) was performed on  
268 such beds. An infiltrated hybrid bed and a clean hybrid bed can be compared by  
269 focusing only on the effect of fine sediment presence and by excluding the potential  
270 effects of changes in bed arrangement.

271 For the preparation of H-G/FS and H-G/Ms beds, a fine sediment-laden flow  
272 recirculated along the flume under flow conditions yielding no gravel motion. For  
273 these beds, the  $D_{15}/d_{85}$  ratio, representing the capacity of the coarsest fine grains  
274 ( $d_{85}$ ) to get through the finest coarse grains ( $D_{15}$ ), was larger than 150. According  
275 to Gibson et al. (2009), USP is the expected infiltration mechanism for  $D_{15}/d_{85} \geq$   
276 15.4, meaning that fine sediments should fill the beds from the bottom upwards.  
277 This was indeed verified (see the evolution of the infiltration in Figure 3b, lines 2

278 and 4). To keep an approximately constant concentration during the infiltration  
279 phase (step (3b)), bags of fine sediments were added periodically to the water tank.  
280 The infiltration phase stopped when the bed was fully clogged, i.e., when gravel  
281 matrix pores were fully filled by fines. The flow discharge was then cut off and the  
282 bed was carefully drained.

283 A similar protocol was used to prepare a H-G/S bed, except during the infil-  
284 tration phase (step (3b)). The sand was too coarse to recirculate mixed with the  
285 water. Therefore, a feeding system located at the flume entrance supplied sand con-  
286 tinuously and uniformly across the channel width. During step (3b), sand moved as  
287 bedload along the flume. Sand particles entered the gravel matrix but were quickly  
288 trapped within the gravel pore spaces near the bed surface, thereby blocking in-  
289 filtration deeper into the substrate and creating a bridge (or seal). This behavior  
290 is consistent with the findings reported by Gibson et al. (2009) who stated that  
291 bridging should occur for  $D_{15}/d_{85} \leq 10.6$  (for the present H-G/S bed,  $D_{15}/d_{85}$  was  
292 equal to 4.5). Step (3b) was stopped when a sand bridge at the surface was stable  
293 along the entire flume length. Flow and sand feedings were cut off and the bed was  
294 carefully drained.

295 **Sediment transport experiment on infiltrated beds** - For the H-G/FS  
296 experiment, the stepped hydrograph and the bedload sampling time were similar  
297 to those used for the clean gravel bed experiments (L-G and P-G). For the other  
298 infiltrated beds, the protocol for the sediment transport experiments was slightly dif-  
299 ferent. For the H-G/Ms experiments, the maximum flow magnitude was increased  
300 because the presence of Ms particles reduced the gravel rate. For the H-G/S experi-  
301 ment, the steady flow plateaus were reduced in time (8 min instead of 15 or 20 min)  
302 and magnitude (see supplementary files) because sand increased the gravel trans-  
303 port. Reducing the duration of each flow plateau prevented significant bed changes.  
304 Bedload was measured at the downstream end of the flume every 4 min. During this  
305 experiment, sand was fed at the same rate as the infiltration phase. For the H-G/FS  
306 and H-G/Ms experiments, fines recirculated at the same concentration as the end

307 of the infiltration phase.

## 308 Results

### 309 Bedload rate over clean gravel beds

310 Figure 5 shows the temporal variation of flow and bedload rates for the L-G-7  
 311 test, which is representative of all tests carried out with L-G and P-G beds (see  
 312 supplementary files); the results differ only in terms of bedload intensity, which  
 313 depends on the initial surface bed arrangement. The bedload rate  $q_s$  increases  
 314 and decreases with flow discharge, following a single-peak shape. At each of the  
 315 hydrograph plateaus, the first of the three measured bedload rates is often the  
 316 highest one (Figure 5), particularly during the rising limb period. This may reflect  
 317 the temporal variability and the beginning of the decline observed in many studies  
 318 at a constant flow discharge (Hassan et al., 2006; Recking et al., 2012; Guney et al.,  
 319 2013).

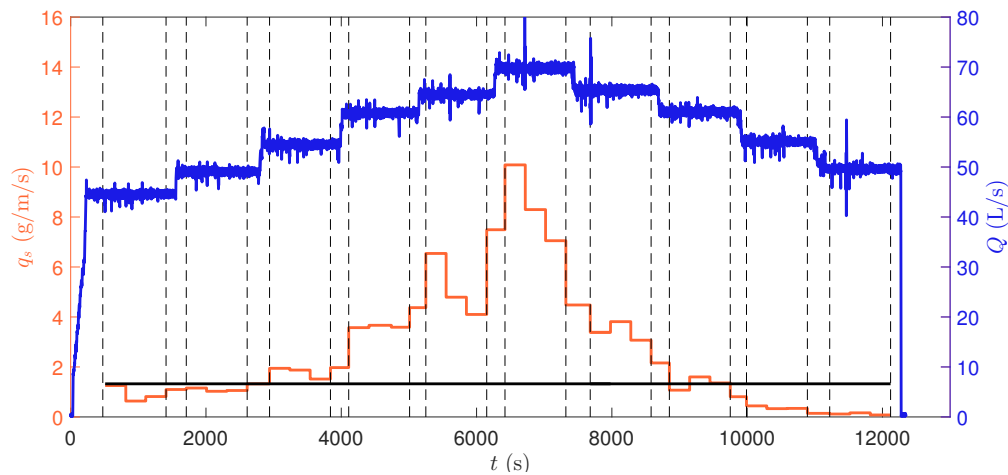


Figure 5: Time variations of bedload rates (in orange) and flow (in blue); results for L-G-7 test. Grid delimits steady states from transition zones. Black horizontal line corresponds to the reference transport rate  $q_{s\text{-ref}} = 1.325 \text{ g.m}^{-1}.\text{s}^{-1}$ .

320 The evolution of the dimensionless bedload rate  $q_s^* = q_s / \sqrt{(s-1)gD_{50}^3}$  as a  
 321 function of the dimensionless bed shear stress  $\tau^* = \tau / [(\rho_s - \rho)gD_{50}]$  (where  $\tau =$   
 322  $\rho g R_h J$  is the bed shear stress,  $s = \rho_s / \rho$  is the relative grain density,  $\rho$  and  $\rho_s$  are the

323 water and sediment density, respectively,  $g$  is the gravitational acceleration,  $R_h$  is the  
 324 hydraulic radius corrected for side-wall effects following the method of Vanoni and  
 325 Brooks (1957),  $J$  is the energy slope set at the bed slope for uniform flow and  $D_{50}$   
 326 is the representative median diameter of gravel particles present on the bed surface)  
 327 is examined in Figure 6.  $D_{50} = 6.8$  mm was assumed for all the calculations, even  
 328 for packed beds, because significant surface grain coarsening was not observed.

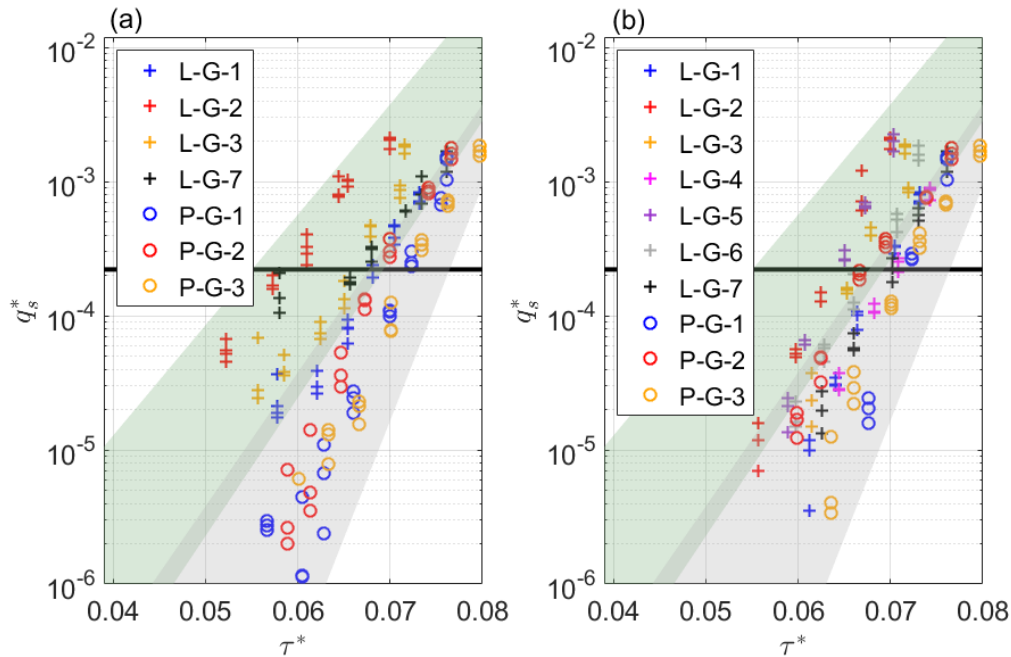


Figure 6: Evolution of the dimensionless bedload rate with dimensionless bed shear stress; results for the clean L-G and P-G beds: (a) at the rising limb and (b) at the falling limb. Green and grey shaded areas delimit loose bed data and packed bed data, respectively, during the rising limb. These areas are reported on Figure 6b. Black horizontal line corresponds to  $q_{s\text{-ref}}^* = 2.2 \times 10^{-4}$ .

329 For the sake of clarity, the bedload rates during flow transitions are not shown in  
 330 Figure 6. The results related to rising and falling limbs are separated to capture any  
 331 possible differences in bedload evolution. Three or four  $q_s^*$ -values are available for a  
 332 given  $\tau^*$ -value (i.e., given flow discharge). At very low bed shear stresses, the bed-  
 333 load fluctuated substantially, making high-accuracy measurements delicate (Ancy  
 334 et al., 2015). The inter-comparison of tests at very low bed shear stress is therefore  
 335 not appropriate. The dimensionless reference transport rate  $q_{s\text{-ref}}^*$  associated with  
 336 the reference transport rate  $q_{s\text{-ref}} = 1.325 \text{ g.m}^{-1}.\text{s}^{-1}$ , defined in the protocol as the

337 gravel's incipient motion, is shown.  $q_{s\text{-ref}}^* = 2.2 \times 10^{-4}$  corresponds to the lowest, suf-  
338 ficiently accurate, measured dimensionless bedload rate. Above this reference rate,  
339 the scatter of  $q_s^*$  is reduced and comparisons between the diverse experiments are  
340 possible (Figure 6). It should be noted that  $q_{s\text{-ref}} = 1.325 \text{ g.m}^{-1}.\text{s}^{-1}$  is larger than  
341 the reference rate calculated from the dimensionless parameter ( $W^* = q^*/\tau^{*3/2}$ )  
342 proposed by Parker et al. (1982). According to these authors, the incipient motion  
343 for gravel particles is attained for  $W^* = 0.002$ , namely with  $q_s$  around  $0.2 \text{ g.m}^{-1}.\text{s}^{-1}$   
344 in the present experiments. This rate is too low and ought to be subjected to large  
345 measurement uncertainty. Retaining  $q_{s\text{-ref}} = 1.325 \text{ g.m}^{-1}.\text{s}^{-1}$  leads to  $W^* = 0.01$  in  
346 the present tests.

347 Figure 6 shows that loose and packed beds behave differently. For a given  $q_s^*$ -  
348 value,  $\tau^*$  is globally lower for loose beds than for packed beds, particularly during the  
349 rising limb. Comparing one *experiment couple* during the rising limb, the reference  
350 dimensionless bed shear stress  $\tau_{\text{ref}}^*$  (i.e., the dimensionless bed shear stress needed  
351 for generating the bedload rate  $q_{s\text{-ref}}^*$ ) for the packed bed can be from 5% to 19%  
352 higher than for the loose bed (on average 12%). We expected that all the data would  
353 collapse for one type of bed (either L-G or P-G) since the same protocol was applied.  
354 However, there are significant differences between two L-G experiments (see L-G-  
355 1 and L-G-2, for example) and they cannot all be explained by the measurement  
356 uncertainty. We believe that the initial bed arrangement is the main cause for  
357 these differences. Nevertheless, two main areas encompass all data related to L-G  
358 experiments (green shaded area) and data related to P-G experiments (grey shaded  
359 area), respectively (see Figure 6a). The scatter due to the temporal variability  
360 of bedload (several  $q_s^*$ -values for one given  $\tau^*$ -value) does not question these two  
361 distinct areas. The intersection of these areas provides a location for data related  
362 to tests on a slightly packed bed. During the falling limbs (Figure 6b), there are  
363 fewer differences between loose and packed beds than during the rising limb. The  
364 reference dimensionless bed shear stress  $\tau_{\text{ref}}^*$  decreases for P-G beds and increases for  
365 L-G beds. The data tend to gather in a single area: the intersection area mentioned

366 above. This behavior characterizes hybrid beds. Somehow, the hydrograph seems  
367 to reset previous shear stress histories, so that both hybrid beds resulting from a  
368 loose or a packed bed present similar bedload dynamics and similar bed surface  
369 arrangements.

370 Bedload hysteresis patterns are observed for both bed configurations (Figure 6).  
371 Clockwise hysteresis (i.e., bedload rates that are larger during the rising limb than  
372 during the falling limb for the same shear stress) are observed for L-G beds, but  
373 either no hysteresis or counter-clockwise hysteresis are noted for P-G beds. These  
374 results reveal a close connection between bedload rate and gravel bed arrangement.  
375 Figure 7 illustrates the hysteresis patterns for the experiment couple n°2, namely  
376 a clockwise loop for L-G-2 and a counter-clockwise loop for P-G-2. For L-G beds,  
377 gravel particles are easily transported during the rising limb while re-arranging and  
378 strengthening the bed. Consequently, bedload rates become lower during the falling  
379 limb. For P-G beds, the opposite behavior is observed. The bed is initially packed  
380 and the gravel transport is initiated for higher bed shear stresses. During the rising  
381 limb, grain structures can be broken and the bed surface can become weak if the bed  
382 shear stress reaches sufficient values. In that case, the mobility of gravel is enhanced  
383 during the falling limb. Otherwise, bedload remains approximately the same during  
384 the falling and rising limbs.

## 385 **Bedload rate over infiltrated beds**

386 Figure 8 presents data related to infiltrated bed experiments and shows the evolution  
387 of  $q_s^*$  with the dimensionless shear stress  $\tau^*$ . Previous areas defined for clean gravel  
388 beds (Figure 6) are recalled in Figure 8 for comparison.

389 During the rising limb, bedload rates for the H-G/FS bed are similar to those  
390 observed during the falling limb for L-G beds (close to the intersection area), indicat-  
391 ing that FS has no influence on gravel dynamics. However, during the falling limb,  
392 the H-G/FS bed behaves differently. Data remain in the same area as during the  
393 rising limb, but  $\tau_{ref}^*$  is smaller. The evolution of bedload follows a counter-clockwise

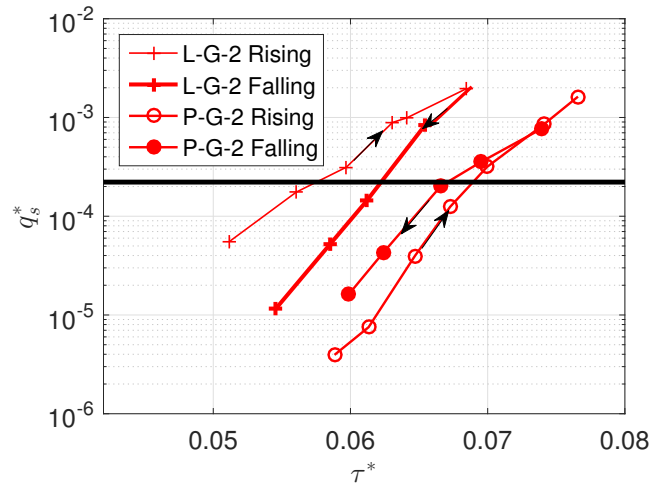


Figure 7: Bedload hysteresis patterns for L-G-2 and P-G-2. Black arrows indicate the hysteresis direction. Black horizontal line corresponds to  $q_{s\text{-ref}}^* = 2.2 \times 10^{-4}$ . The bedload rates presented here correspond to values averaged over each steady plateau.

394 loop, which was not the case for L-G experiments. The gravel transport during the  
395 falling limb was thus enhanced compared to the rising limb: FS was rapidly washed  
396 from the bed surface and progressively from the substrate. At the falling limb, FS  
397 reached a sufficient concentration within the water column to result in a gravel-fine  
398 interaction. FS sediments affect bedload during the falling limb by lubricating the  
399 bed.

400 Results for the H-G/Ms beds gather in the area that previously corresponds  
401 to P-G bed data during the rising limb (Figure 8a). In our case, clogging with  
402 cohesive Ms has similar effects on bed mobility as gravel arrangement. In addition,  
403 data from H-G/Ms-6 have the same behaviour than the other data from H-G/Ms  
404 experiments, even if the bed resulted from an initial P-G bed. The lack of difference  
405 within hybrid beds is once again verified. Data from H-G/Ms tests follows counter-  
406 clockwise hysteresis, meaning that the transport of gravel is enhanced during the  
407 falling limb, except in the H-G/Ms-5 test that shows a clockwise hysteresis. This  
408 exception will be discussed in the Discussion Section. During the rising limb, Ms is  
409 more difficult to wash out of the bed surface than FS because of its cohesion. Gravel  
410 mobility is reduced due to the presence of cohesive Ms. During the falling limb, the  
411 infiltrated gravel bed is partially cleaned from Ms, and then tends to behave like a

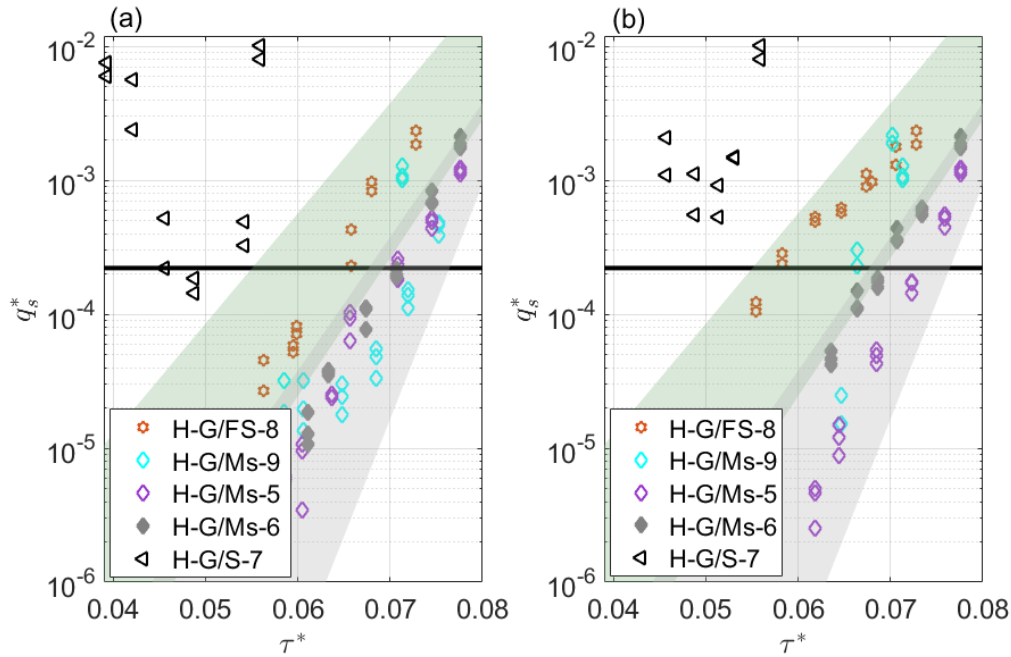


Figure 8: Evolution of the dimensionless bedload rate with dimensionless bed shear stress; results for infiltrated gravel beds: (a) at the rising limb and (b) at the falling limb. Green and grey shaded areas are the same as presented in Figure 6. The open and closed symbols denote data obtained on hybrid beds resulting from initial loose and packed beds, respectively. Black horizontal line corresponds to  $q_{s\text{-ref}}^* = 2.2 \times 10^{-4}$ .

412 clean H-G bed.

413 For the gravel bed infiltrated with sand (H-G/S-7), the highly scattered bedload  
 414 rates make the results difficult to interpret. Figure 8 shows a new area for the H-G/S  
 415 experiment, with high bedload rates for  $\tau^*$ -values being much lower than those for  
 416 the other experiments. The seal of sand clearly enhanced the gravel transport. No  
 417 hysteresis loop is identifiable and no single  $\tau_{\text{ref}}^*$  could be defined during the rising  
 418 and falling limbs. Figure 9 shows the evolution of bedload as a function of time and  
 419 hydraulic conditions, to be compared to Figure 5 (L-G-7 test). Contrary to L-G-7,  
 420 bedload evolution in H-G/S-7 shows a two-peak shape (Figure 9). The first bedload  
 421 peak observed at very low flow discharges is probably caused by the presence of  
 422 the bridge of sand lubricating the bed surface. The second peak appears at a flow  
 423 discharge of around 60 L/s, similar to the increase in bedload for L-G-7 (Figure 5).  
 424 However, the bedload rate is six times higher when sand is present.

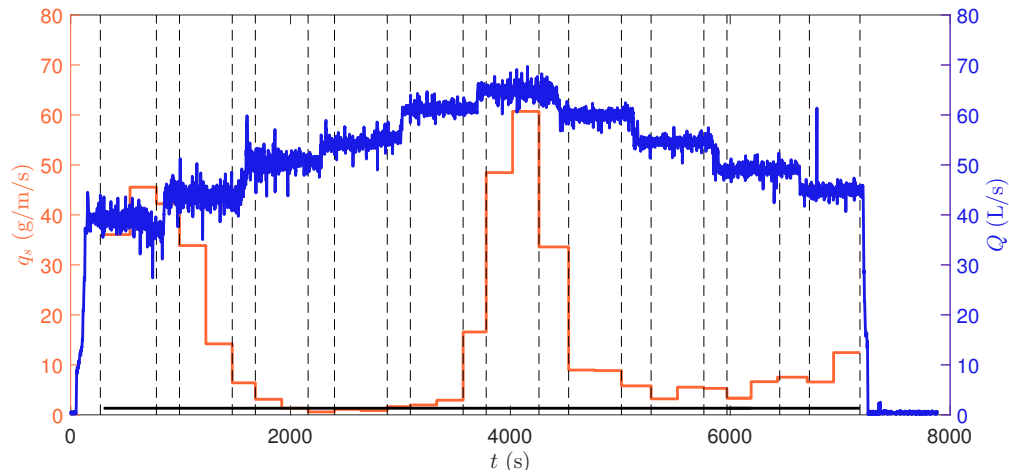


Figure 9: Time variations of bedload rates (in orange) and flow (in blue); results for the H-G/S-7 test. Grid delimits steady states from transition zones. Black horizontal line corresponds to  $q_{s\text{-ref}} = 1.325 \text{ g.m}^{-1}.\text{s}^{-1}$ .

## 425 Summary of the results

426 Figure 10 shows a schematic temporal evolution of different beds responding to  
 427 similar bed shear stresses. This Figure highlights significant steps generating sub-  
 428 substantial changes in the bed matrix composition and in sediment transport ( $T0$ - $T5$ ).  
 429 In one line, the absence of a box means that no significant change occurred between  
 430 the time considered and the previous time. Values of  $\tau_{\text{ref}}^*$  are represented with hor-  
 431 izontal bold color lines and plotted on the evolution graph ( $\tau^*$ ,  $t$ ) for each type of  
 432 bed. Each color is associated with one specific bed (see colors of the box edges).  
 433  $\tau_{\text{ref-R}}^*$  corresponds to the dimensionless bed shear stress for which the initiation of  
 434 motion during the rising limb was observed and  $\tau_{\text{ref-F}}^*$  corresponds to the dimension-  
 435 less bed shear stress for which the cessation of sediment motion was observed during  
 436 the falling limb. The bed arrangement and degree of clogging described at  $T5$  refer  
 437 to the final bed state ( $T_f$ ).

438 **Loose and packed beds (L-G and P-G)** - A loose bed is put into motion  
 439 ( $T2$ ) before a packed bed ( $T3$ ) (red and black boxes in Figure 10). For the L-G  
 440 bed,  $q_s$  is higher than the reference value  $q_{s\text{-ref}}$  between  $T2$  and  $T5$ . During this  
 441 time lapse, the L-G bed packs and organizes itself. The resulting bedload rate  
 442 during the falling limb is lower than during the rising limb for the same bed shear

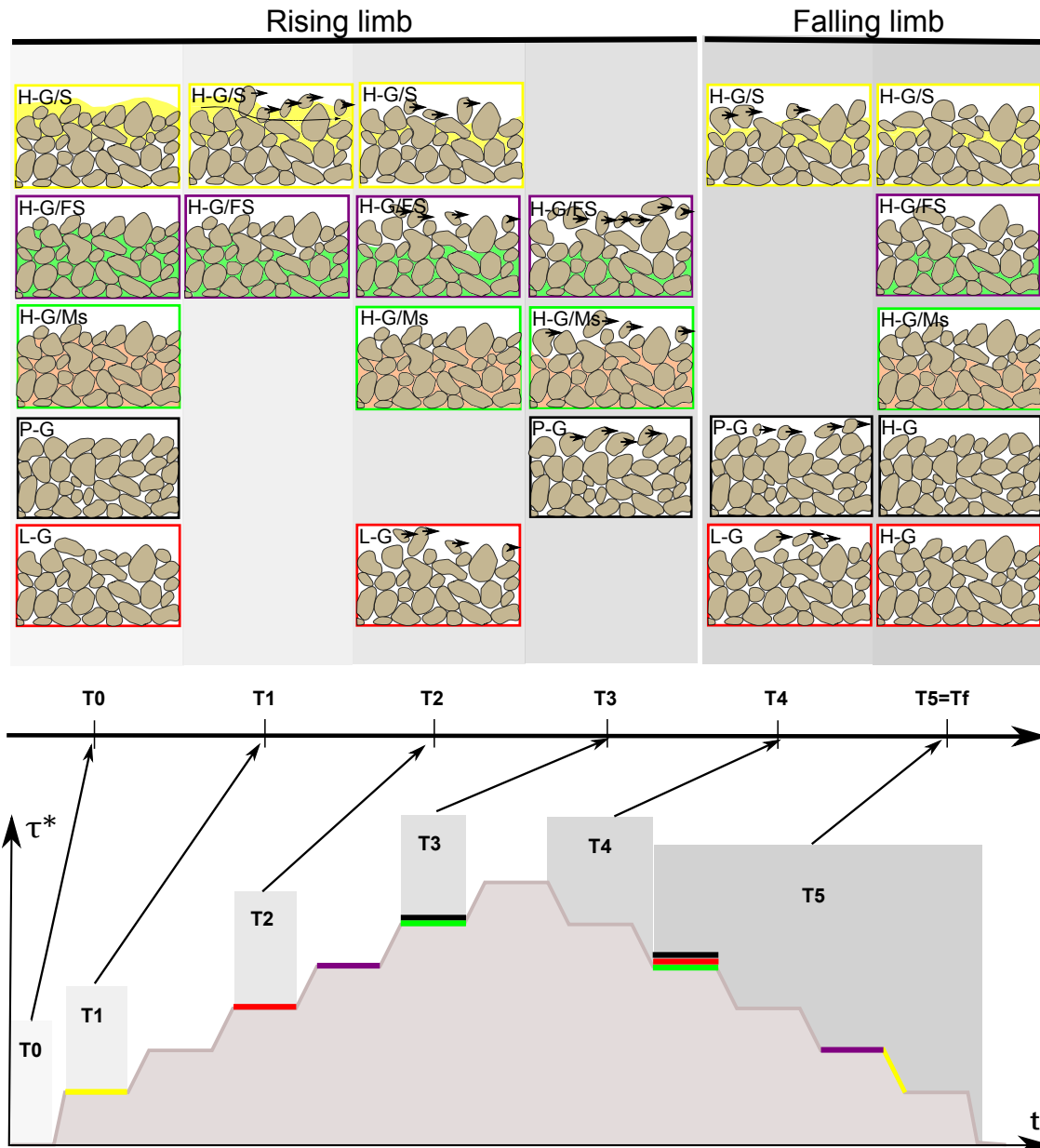


Figure 10: Description of the different bed evolutions during a hydrograph. Each line in the upper part describes how a specific bed evolves during the hydrograph schematized below. A color is attributed to each bed type (contour of the box). Key times in this evolution are denoted  $T_0$  to  $T_5$  and represented by shaded columns on both hydrograph and upper part of the diagram. A missing box in the line means that no change occurred between the time considered and the previous time. Horizontal color lines on the hydrograph correspond to  $\tau_{\text{ref-R}}^*$  and  $\tau_{\text{ref-F}}^*$  for each bed type. Arrows inside the boxes represent gravel transport. They are not scaled according to the sediment transport intensity.

443 stress (clockwise hysteresis). The opposite is observed for the packed bed (counter-  
444 clockwise hysteresis), meaning that the flow has probably started to break grain  
445 arrangements initially present on the bed surface ( $T3 - T4$ ). The final states of both  
446 beds tend to become similar as well as the reference dimensionless bed shear stress  
447  $\tau_{\text{ref-F}}^*$ . A hybrid bed H-G is obtained.

448 **Beds infiltrated with Ms (H-G/Ms)** - The following description of the H-  
449 G/Ms behaviour is suitable for both hybrid beds resulting from an initial loose bed  
450 or packed bed. At the beginning of the rising limb ( $T0 - T1$ ), gravel particles forming  
451 the H-G/Ms bed (green boxes) are totally enclosed by fine consolidated sediments.  
452 The bed surface layer of the matrix is first washed of its fine sediments ( $T2$ ). At  $T3$ ,  
453 gravel is transported at the same  $\tau_{\text{ref-R}}^*$  as the P-G bed while fine sediments are still  
454 washed from the bed. In our experiments, cementation and packed arrangement  
455 have effects of similar magnitude on gravel transport. During the falling limb, the  
456 bed behaves in the same way as a H-G bed. At  $T5$ , the H-G/Ms bed surface tends  
457 to become similar to the H-G bed surface, as well as the associated  $\tau_{\text{ref-F}}^*$ .

458 **Beds infiltrated with FS (H-G/FS)** - During the rising limb, a H-G/FS bed  
459 (purple boxes) evolves similarly to a H-G bed, because fines are easily and quasi-  
460 instantaneously ( $T1$ ) washed out of the bed surface. As the  $\tau^*$  peak is reached, FS is  
461 preferentially put into suspension, causing an increase in fine sediment concentration  
462 into the flow ( $T3$ ). It is important to recall that FS was recirculated with water.  
463 This high concentration lubricates the bed surface, enhancing the gravel transport  
464 ( $T3 - T4$ ). The shape of FS is spherical (Figure 2), which may favor this lubrication.  
465 During the falling limb, no strong organization is observed. The significant gravel  
466 transport prevents particle organizations. If conditions of low bedload were longer,  
467 grain organizations might appear. At  $Tf$ , the bed surface is significantly loose with  
468  $\tau_{\text{ref-F}}^*$  lower than in the other cases described above.

469 **Beds infiltrated with S (H-G/S)** - As shown in Figure 9, the bedload evo-  
470 lution for the H-G/S bed (yellow boxes) is marked by two main stages. First, at  
471 low-flow discharge during the rising limb ( $T1$ ), the bed surface is highly concentrated

472 in sand, which lubricates and facilitates gravel particles rolling around their neigh-  
473 bours. The equal mobility phenomenon was observed, meaning that gravel particles  
474 are transported as easily as sand (Parker et al., 1982). The highly concentrated  
475 sand layer starts moving as bedload on the bed surface. The moving sand particles  
476 collide with gravel particles, destabilize them and finally entrain them. As the sand  
477 layer is washed from the bed surface, gravel transport decreases. Although there  
478 was sand feeding during this experiment, it was not sufficient to maintain a high  
479 concentration at the surface layer; consequently the gravel transport rate decreased.  
480 Once  $\tau^*$  reaches the reference value  $\tau_{\text{ref-R}}^*$  found for the L-G tests, significant gravel  
481 transport is observed again (*T2*). Even if the sand concentration infiltrated into the  
482 bed is relatively low compared to what was on the bed surface at the beginning of  
483 the experiment, it is still high enough to enhance the transport of gravel (*T3-T5*).  
484 The intensity of this effect may be attributed to the fact that sand and gravel are  
485 mainly transported as bedload.

## 486 Discussion

### 487 Impact of bed arrangement

488 Under similar hydraulic conditions (see supplementary files), diverse bedload rates  
489 were observed for beds composed with the same material (same GSD) having differ-  
490 ent levels of arrangements. The arrangements of L-G and P-G beds were quantified  
491 using the laser scanner. The analysis of the three-dimensional topographic surveys of  
492 the bed surfaces revealed substantial changes between the two types of bed (Marion  
493 et al., 2003; Mao et al., 2011; Perret et al., 2016).

494 The geometrical grain roughness of the bed surface ( $\sigma_{zg}$ ) was found to be smaller  
495 for P-G beds than for L-G beds, revealing a better bed surface particle imbrication  
496 and thus a smoother bed surface for packed beds. Small bedforms (preferential  
497 pathways) and bed structures were present on P-G bed surfaces. Structure lengths  
498 in the streamwise ( $\Delta_{x0}$ ) and the cross-stream direction ( $\Delta_{y0}$ ) were about  $2 \times D_{50}$ .

499 Gravel particles were orientated in the streamwise direction for P-G beds, whereas  
500 they were randomly organized in L-G beds (Nikora et al., 1998; Marion et al., 2003).  
501 The drag force for gravel orientated in the streamwise direction is on average smaller  
502 than for randomly orientated gravel. In addition, a decrease in bed surface roughness  
503 should lead to lower flow resistance as well (Smart et al., 2002). Gravel transport  
504 should therefore be reduced for the P-G experiments in comparison to the L-G  
505 tests considering the same hydraulic conditions. This is consistent with our results  
506 (see Figure 6). Topographic surveys made at the end of each sediment transport  
507 experiments were also analyzed and showed that bed surfaces were quite similar for  
508 hybrid beds (resulting from a loose or a packed bed) in terms of bed roughness,  
509 imbrication and grain orientation.

510 We have seen that results from loose and packed beds at the falling limb (i.e.  
511 hybrid beds, see Figure 6) form a scattered data set among which both beds can not  
512 be distinguished. The lengths of the bed forms at the end of the experiments show  
513 also a significant scatter. This scatter is nevertheless lower for the grain roughness,  
514 which is the source of skin friction. It should be recalled that the total bed shear  
515 stress  $\tau$  can be broken down into a bed shear stress component due to grain resis-  
516 tance,  $\tau_g$ , and a bed shear stress component due to form resistance,  $\tau_f$ . Sediment  
517 motion is generally attributed to the skin friction  $\tau_g$  and not to the total shear stress  
518  $\tau$  (Petit et al., 2015). To further investigate the part of bed forms in the scatter of  
519 our data and focus on grain scale, we estimate the skin friction to analyse sediment  
520 transport rate in our experiments.

521 Figure 11 shows  $q_s^*$  as a function of  $\tau_g^*$ , computed using the Manning-Strickler  
522 equation and a Strickler coefficient  $K_g = 21/D_{50}^{1/6}$ , which represents skin roughness  
523 assumed to be identical for all experiments conducted on clean beds:

$$\tau_g = \rho g \left( \frac{Q}{W \sqrt{J} K_g} \right)^{3/5} J \quad (1)$$

524 where  $W$  is the channel width.

525 The same trend as in Figure 6 is replicated in Figure 11, namely two dimension-

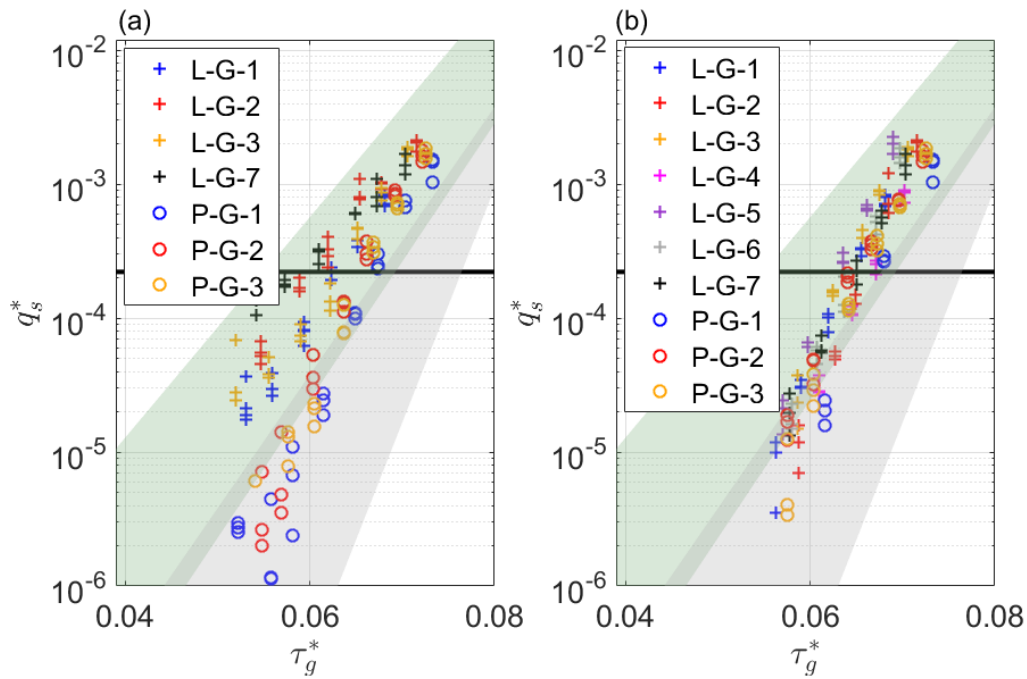


Figure 11: Evolution of the dimensionless bedload rate with dimensionless skin friction: (a) rising and (b) falling limbs data. Gray and green shaded areas are the same as in Figure 6. Black horizontal line corresponds to  $q_{s\text{-ref}}^* = 2.2 \times 10^{-4}$ .

526 less bed shear stress zones are present during the rising limb versus one area during  
 527 the falling limb. Assuming the same bed roughness for all the clean beds during  
 528 the falling limb seems reasonable. Indeed, the scatter is reduced and data are closer  
 529 to a single curve. During the falling limb, the beds have a similar flow history and  
 530 bed surface arrangement (verified with the scanner surveys). During the rising limb,  
 531 differences are still present between the beds, even ignoring the bed form effect on  
 532 flow resistance (Figure 11a). This could indicate that the hypothesis of similar bed  
 533 roughness is inappropriate and that the estimation of  $\tau_g$  with a single bed roughness  
 534 coefficient is probably mistaken. In addition, changes in bed arrangement may not  
 535 influence only flow resistance, but also bed stability defined by the distributions  
 536 of the dislodging forces, which individual grains can resist before moving (Tait,  
 537 1993). Bed stability is assessed by bed roughness and additional indicators such as  
 538 the lengths of bedforms and structures, the degree of armoring ( $A_r$ ) (Cooper and  
 539 Tait, 2009) and the main orientation of the bed surface grains ( $\Phi$ ) (Friedrich, 2010).  
 540 The analysis of the laser scanner surveys supports the hypothesis of an incorrect  
 541 estimation of  $\tau_g$ , but does not inform on the impact of bed arrangement on bed

542 stability.

543 In bedload prediction models, flow resistance and bed mobility are often rep-  
544 resented using hydraulic roughness ( $k_s$ ) and a criterion defining the gravel's in-  
545 cipient motion ( $\tau_{ref}^*$ ), respectively (Wilcock et al., 2009). Improving these models  
546 requires assessing changes in both flow resistance and bed stability. Regarding the  
547 experimental results reported herein, both  $\tau_{ref}^*$  and  $k_s$  seem sensitive to change in  
548 bed arrangement. They are therefore at least dependent on a combination of sev-  
549 eral indicators of bed surface arrangement, e.g.  $k_s = f(\sigma_{zg}, \Delta_{x0}, \Delta_{y0}, A_r, \Phi, \dots)$  and  
550  $\tau_{ref}^* = f(\sigma_{zg}, \Delta_{x0}, \Delta_{y0}, A_r, \Phi, \dots)$ .

551 We were not able to explain the link between  $q_s$  and bed arrangement parameters  
552 exhaustively, nor to reduce the number of controlling parameters. For this to be  
553 achieved, supplementary data are needed. Nevertheless, some correlations were  
554 found between  $\tau_{ref}^*$  and bed surface indicators, helping to understand the impact of  
555 bed arrangement on bedload transport, such as the correlation between the decrease  
556 in  $\tau_{ref}^*$  and the decrease in geometrical grain roughness, the correlation between  
557 the increase in  $\tau_{ref}^*$  and the increase in bedform heights, structure lengths and bed  
558 armoring degree, the correlation between the increase in  $\tau_{ref}^*$  and the appearance  
559 of a preferential grain orientation. Figure 12 illustrates some of these observed  
560 correlations.

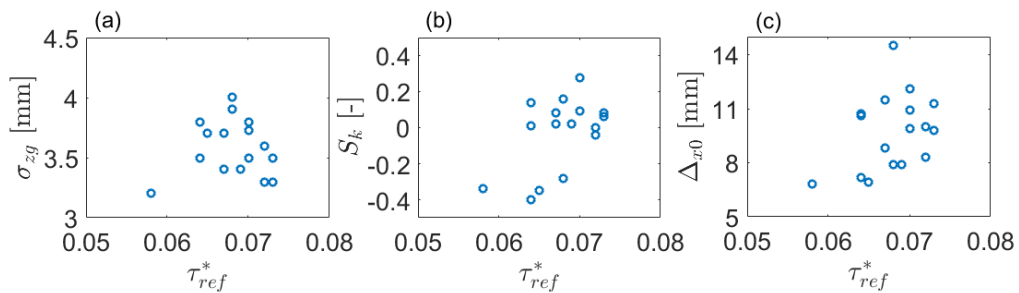


Figure 12: Relation between dimensionless reference bed shear stresses and their associated bed surface indicators. Bed surface parameters are (a) geometrical grain roughness or (b) bed armoring degree or (c) the length of the bed surface structures in the flow direction.

## 561 **Impact of geotechnical bed properties**

562 Our observations revealed that the presence of infiltrated fine sediments needs to be  
563 taken into account when studying bedload dynamics.

564 Tests were performed on beds infiltrated from the bottom up with fine sediments  
565 having similar grain sizes but different geotechnical properties (H-G/FS and H-  
566 G/Ms). The results showed that fine sediments affected gravel mobility differently.  
567 In presence of Ms,  $q_s$  was reduced, whereas in presence of FS,  $q_s$  was enhanced for  
568 similar bed shear stress. The size of the fines is therefore not the only parameter  
569 to be considered when studying infiltrated beds. The geotechnical properties of the  
570 gravel matrix can change depending on the type of infiltrated fine sediments (Table  
571 1). Bed permeability, consolidation and fine sediment shape are also important  
572 parameters controlling  $q_s$ .

573 Bed permeability  $k$  mainly depends on the grain size and particle shape of the  
574 coarse and fine particles. Previous studies highlighted the impact of bed permeability  
575 on hydraulic roughness (Manes et al., 2009; Hamm et al., 2011). Hamm et al. (2011)  
576 measured bed shear stresses in open-channel flows over permeable beds formed by  
577 glass beads ( $D_{50} = 1.5$  mm) or cobbles ( $D_{50} \approx 6.5$  cm). They found that bed shear  
578 stresses were 1.5-2 times greater than those for impermeable beds under equivalent  
579 hydraulic conditions. This effect was attributed to the momentum balance associ-  
580 ated with water exchange across the sediment-water interface (Manes et al., 2009).  
581 This increase in bed shear stress facilitates sediment movement for permeable beds.  
582 In permeable beds, the bed shear stress is distributed over a finite depth instead of  
583 a surface as in an impermeable bed. The observation of the in-bed water velocity  
584 profile suggests that this depth is limited to one or two grain diameters and that  
585 most of the shear stress is applied on grains of the first bed surface layer (Leonard-  
586 son, 2010). In impermeable beds, the bed shear stress acts predominantly on the  
587 upper part of the surface grain, whereas in the case of permeable beds, it acts on  
588 the whole grain, therefore enhancing grain motion. In our case, beds infiltrated with  
589 fine sediments from the bottom up have similar bed permeabilities, which are much

590 smaller than in the case of L-G beds (Table 1). Permeability Reynolds numbers  
591 ( $Re_k = \sqrt{k}u^*/\nu$ ) are less than 1, indicating that these beds will behave as if they  
592 were impermeable (Breugem et al., 2006; Manes et al., 2009). On the contrary, L-G  
593 beds are considered as permeable beds (high values of  $Re_k$ ). Gravel mobility should  
594 be reduced on H-G/Ms and H-G/FS beds compared to L-G beds. However, Figure  
595 8 shows that this was not always the case. If L-G beds (permeable) were put into  
596 motion more easily than H-G/Ms beds (impermeable), the opposite behavior dur-  
597 ing the falling limb was observed between L-G beds (permeable) and H-G/FS beds  
598 (impermeable). Therefore, other factors than bed permeability may also control the  
599 bedload rate.

600 The decreased erodibility of a H-G/Ms bed can be attributed to a change in bed  
601 stability due to the higher consolidation caused by the presence of fine sediments  
602 (see  $C_u$  in Table 1). The H-G/FS bed was not consolidated ( $C_u = 0$ ) compared to  
603 beds formed with Ms. The latter consolidates the gravel matrix and prevents gravel  
604 from moving. It is important to recall that  $C_u$  increases with the decrease in water  
605 content within the bed, which depends on the residence time of fine sediments. This  
606 residence time ( $T_r$ ) corresponds to the time during which the fines were present in  
607 the drained gravel matrix before the beginning of the sediment transport experiment  
608 (see Figure 4, the time between steps (3b) and (4)). The longer this time is, the less  
609 erodible the bed material is. Indeed, H-G/Ms beds with the longest  $T_r$  are those  
610 with the lowest bedload rate ( $T_r$  equal 12, 5 and 3 days for H-G/Ms-5, H-G/Ms-6  
611 and H-G/Ms-9, respectively) (Figure 8). In this way,  $q_s$  decreases as bed material  
612 consolidation increases. The hysteresis pattern of H-G/Ms-5 showed a clockwise loop  
613 as opposed to the other tests performed with Ms. This difference can be explained  
614 by remarkably high bed consolidation. During the rising limb, the flow removed fines  
615 from the first surface layer, while transporting some gravel particles. Then the flow  
616 encountered strongly consolidated fine sediments located on the subsurface where  
617 gravel is totally enclosed by Ms. Fine sediments present on the bed surface were  
618 easier to de-clog than those present in the subsurface. That is why a reduction in the

619 bedload rate occurred during the falling limb of the hydrograph. The residence time  
620 of fine sediments  $T_r$  appears to be an important parameter for predicting bedload  
621 rate.

622 The difference in bedload rate between the H-G/Ms and H-G/FS bed experi-  
623 ments may also be related to the shape of fine sediments. Several authors have  
624 investigated the effect of coarse sediment shape on bed shear stress (Li and Komar,  
625 1986; Durafour et al., 2015). They found that particles with non-spherical shapes  
626 (flat, angular or elongated) have stronger imbrication patterns than spherical par-  
627 ticles. Li and Komar (1986) showed that the bed shear stress required to put into  
628 motion non-spherical material might be up to six times greater than the bed shear  
629 stress for moving spherical grains. Durafour et al. (2015) observed that changes in  
630 bed shear stress were controlled by changes in the sediment circularity index ( $C_I$ ).  
631 Transposing these findings for coarse particles to fine particles used in this study  
632 could explain why H-G/FS beds were easier to move than H-G/Ms beds. Ms par-  
633 ticles ( $C_I = 0.75$ ) contribute to consolidating the bed because of their angular and  
634 elongated shapes, reducing the sediment transport in contrast to spherical FS parti-  
635 cles ( $C_I = 0.99$ ) (Table 1). The significant dispersion of the GSD of the medium silt  
636 (Figure 2) probably also reduces the porosity and enhances the bed consolidation.  
637 The increase in erodibility of the H-G/FS bed may be attributed to a decrease in  
638 bed stability due to the lubrication effect of the circular FS washed out of the gravel  
639 matrix.

## 640 **Importance of fine sediment concentration**

641 Tests were performed on beds infiltrated with non-cohesive fine sediments having  
642 different grain sizes (H-G/FS and H-G/S). In both cases, the gravel mobility was  
643 enhanced, but to a lesser extent in the H-G/FS experiment.

644 Previous studies showed that gravel transport increased in presence of non-  
645 cohesive fine sediments within the bed (Jackson and Beschta, 1984; Wilcock et al.,  
646 2001; Curran, 2007; Koll and Dittrich, 2010). This increase is often associated with

647 a reduction of the mean grain diameter characterizing the overall bed (Hill et al.,  
648 2017). In our case, the bedload rate was higher in the presence of sand than in the  
649 presence of fine sand. Yet, the mean grain diameter of the bed was lower for the  
650 H-G/FS bed than for the H-G/S bed. Therefore, previous indicators might not be  
651 suitable for characterizing gravel transport with infiltrated beds.

652 In the H-G/FS experiment, gravel transport was not influenced by fine sediments  
653 during the rising limb (the results were similar to those found during the falling limb  
654 of the L-G experiments), whereas it increased during the falling limb (Figure 8). Yet,  
655 we expect the GSD of the overall bed surface to increase as part of the fines are  
656 washed out. The increase in sediment transport might be explained by the fact  
657 that between the rising and falling limbs, the fine sediment concentration within  
658 the flow increased due to the re-suspension of fine particles. In their experiments,  
659 Wilcock and Crowe (2003) found that high fine sediment content in the surface  
660 ( $> 30\%$ ) strongly enhances bedload rate. Considering the H-G/FS results, we  
661 believe that fine sediment concentration in the bedload layer  $c_f$  (and not in the  
662 surface) is a controlling parameter for gravel transport. We define the bedload layer  
663 as the thin layer at the bed surface, where gravel particles are transported and where  
664 interactions between fine and coarse sediments occur. The analysis of  $c_f$  can also  
665 explain the difference between the H-G/FS and H-G/S experiments. Indeed, for the  
666 H-G/S experiment, sand moves as bedload resulting in a much higher concentration  
667 in sand within this layer than for the H-G/FS experiment (FS was transported in  
668 suspension).  $c_f$  depends on the transport mode (bedload or suspension) and bedload  
669 rates are higher for higher  $c_f$  such as in the H-G/S experiment. The H-G/S test  
670 also highlights the importance of considering the time variation of  $c_f$  when studying  
671 gravel transport. Knowing the fine sediment distribution within the bed (related  
672 to the type of infiltration) helps predict the temporal evolution of  $c_f$ . We suggest  
673 taking  $c_f(t)$  into account in new bedload models.

## 674 Recommendations for bedload prediction

675 Based on our experiments (Figure 10) and on previous studies (Wilcock and Crowe,  
676 2003; Hassan et al., 2006; Jain and Kothyari, 2009; Recking, 2009), a methodology  
677 for improving bedload prediction in gravel-bed rivers is suggested. In this paper, we  
678 provide clues for estimating  $\tau_{ref}^*$  more accurately, which is a key parameter in bedload  
679 models. Adjusting the  $\tau_{ref}^*$  value according to the bed arrangement and gravel matrix  
680 composition is the base of the methodology. The methodology for predicting the  
681 bedload rate of a specific gravel-bed typically depends on the bedload model used,  
682 and more specifically on the definition of  $\tau_{ref}^*$  in the model.

683 The methodology can be recapped as follows:

- 684 1. Make a first estimate of  $\tau_{ref}^*$  as a function of the chosen bedload formula (e.g.  
685 Meyer-Peter and Müller, 1948) and assume that it corresponds to  $\tau_{ref}^*$  for loose  
686 gravel beds. For example, if  $\tau_{ref}^*$  is assumed equal to the critical dimensionless  
687 bed shear stress  $\tau_{cr}^*$  defined by Shields (1936), one can use the gravel GSD  
688 characteristics and existing diagrams or equations (Yalin and Karahan, 1979;  
689 Soulsby and Whitehouse, 1997) to calculate its value.
- 690 2. Characterize the gravel-bed (i.e., level of bed arrangement, degree of clogging  
691 and type of bed infiltration).
- 692 3. Adjust  $\tau_{ref}^*$  according to bed configuration (from 0 to +12 % according to the  
693 level of arrangement, from 0 to +12 % according to the level of consolidation  
694 and from -40 to 0 % according to the concentration of non-cohesive fine sedi-  
695 ments in the bedload layer). These values are given as an indication and are  
696 based on our laboratory results (Figure 6 and 8). They were calculated using  
697 the percentage difference of  $\tau_{ref}^*$  between experiments from the same couple of  
698 experiments. An average is then made for each type of beds. The percentage  
699 difference can slightly increase if the arbitrary value for  $q_{s-ref}$  is chosen smaller.  
700 However, the trends (i.e. increasing or decreasing  $\tau_{ref}^*$ ) remain the same.
- 701 4. Compute  $q_s$  using the new  $\tau_{ref}^*$  and the related bedload formula.

702 We do not claim that the above methodology provides quantitative values for  $\tau_{\text{ref}}^*$ .  
703 Even if the first estimate of  $\tau_{\text{ref}}^*$  is mistaken, the recommended relative adjustment  
704 should still be valid and coherent. Further studies with different sediments and  
705 hydraulic conditions should be tested to validate the given qualitative ranges of  
706 adjustment. The final bedload trends are in coherence with those found in previous  
707 studies, namely a decrease in  $q_s$  with strong bed arrangement (Hassan et al., 2006;  
708 Guney et al., 2013) and in presence of cohesive fine sediments (Jain and Kothyari,  
709 2009; Barzilai et al., 2013) and an increase in  $q_s$  in presence of non-cohesive fine  
710 sediments (Wilcock and Crowe, 2003; Curran and Wilcock, 2005). In-situ tests were  
711 conducted to verify this methodology (Camenen et al., 2015).

712 Even if the slope effect was not studied in this paper, it could be interesting  
713 to suggest an adjustment as a function of changes in bed slope. Previous studies  
714 found that  $\tau_{\text{ref}}^*$  increases with an increase in bed slope (Chiew and Parker, 1994;  
715 Shvidchenko and Pender, 2000; Mueller et al., 2005; Lamb et al., 2008; Recking,  
716 2009). The bedload rate is then lower at high slopes. The reasons for this decrease  
717 remain only partially explored. In steep flows, the relative roughness ( $k_s/h$ ) is high  
718 and the bed arrangement is strong. Changes in relative roughness impact the flow  
719 structure and turbulence, modifying the bedload rate. The slope effect is actually  
720 a consequence of the linked effects of bed arrangement (Shvidchenko and Pender,  
721 2000) and relative roughness (Lamb et al., 2008; Recking, 2009) that should be taken  
722 into account when predicting the bedload rate.

## 723 Conclusion

724 Original laboratory experiments were conducted to investigate the mobility of gravel  
725 under low bed shear stresses. Particular attention was paid to the roles played by  
726 the gravel surface arrangement and by fine sediments infiltrating the gravel matrix.  
727 A total of 15 experiments were conducted with different bed configurations: clean  
728 loose and packed gravel beds, and gravel beds infiltrated with sand, non-cohesive  
729 fine sand or cohesive medium silt. Unsteady flow conditions ensuring low bed shear

730 stresses were simulated. Laser scanning of the bed topography was performed to  
731 retrieve information on bed changes. The results showed that both the bed ar-  
732 rangement (e.g., structure sizes, degree of bed armoring, surface grain imbrication  
733 and orientation) and the presence of fine sediments (e.g., nature, shape and concen-  
734 tration of fines, degree of bed consolidation) significantly govern the transport of  
735 gravel.

736 The bedload rate decreases with decreasing bed roughness, increasing grain struc-  
737 ture lengths, increasing grain imbrication and with gravel particles preferentially  
738 aligned with the flow direction. The mobility of a packed gravel bed decreases up  
739 to 12 % compared to a loose gravel bed. Cohesive and angular silt infiltrated into  
740 the gravel matrix strongly reduces the bedload rate by consolidating the gravel bed,  
741 thereby increasing the reference bed shear stress up to 12 % compared to a clean  
742 gravel bed. The opposite behavior was observed with non-cohesive and spherical  
743 fine particles, namely gravel bed lubrication due to fine presence and a reduction of  
744 the reference bed shear stress up to 40 % compared to a clean gravel bed. Under  
745 low-flows, the gravel movement can be enhanced if the concentration of fine particles  
746 is high enough in the bedload layer, which is accompanied by a reduction in flow  
747 roughness and turbulence and an acceleration in near-bed flow.

748 We suggest a methodology for improving the computation of bedload rate in  
749 mountain rivers. We recommend adjusting the dimensionless reference bed shear  
750 stress in bedload transport capacity formulae according to the degree of bed surface  
751 arrangement (loose or packed), the presence of fines (concentration in the bed-  
752 load layer) and the characteristics of fines infiltrated into the bed (cohesive or  
753 non-cohesive, grain shape): from 0 % to +12 % depending on the degree of bed  
754 arrangement, from 0 % to +12 % for gravel infiltrated with cohesive and angular  
755 fine particles, and from -40 % to 0 % for gravel infiltrated with non-cohesive fine  
756 particles.

757 The present work is an additional step toward a consistent investigation of gravel  
758 transport in open channels. Further experiments could help build a new bedload

759 model that considers the effect of bed arrangement and gravel matrix composition.  
760 Tests could be conducted under a broader range of flow conditions (e.g., flow hy-  
761 drographs, changing flow directions), channel geometry (e.g., bed slope) and more  
762 complex configurations (e.g., water-worked bed, alternate bars), with various bed  
763 material compositions (e.g., gravel infiltrated with silt/sand mix).

## 764 Acknowledgements

765 The experiments were supported by Irstea, EDF (Electricité de France), the French  
766 Water Agency (AE-RMC) and the OSR research program (Rhône Sediment Obser-  
767 vatory). The Irstea Lyon-Villeurbanne metrology team, especially Alexis Buffet, are  
768 gratefully acknowledged for their technical support in performing the laboratory ex-  
769 periments. The authors would like to thank Sylvie Nicaise (Irstea Aix-en-Provence)  
770 and Khedidja Abbaci (Irstea Lyon-Villeurbanne) for their assistance in the charac-  
771 terization of sediment properties.

## 772 References

- 773 Ancey, C., Bohorquez, P., and Heyman, J. (2015). Stochastic interpretation of the  
774 advection-diffusion equation and its relevance to bed load transport. *Journal of*  
775 *Geophysical Research: Earth Surface*, 120(12):2529–2551. 2014JF003421.
- 776 Barzilai, R., Laronne, J. B., and Reid, I. (2013). Effect of changes in fine-grained ma-  
777 trix on bedload sediment transport in a gravel-bed river. *Earth Surface Processes*  
778 *and Landforms*, 38:441–448.
- 779 Beschta, R. L. and Jackson, W. L. (1979). The intrusion of sediments into a stable  
780 gravel bed. *Journal of the Fisheries Research Board of Canada*, 36(2):204–210.
- 781 Breugem, W., Boersma, B., and Uittenbogaard, R. (2006). The influence of wall  
782 permeability on turbulent channel flow. *Journal of Fluid Mechanics*, 562:35–72.

- 783 Buffington, J. M. and Montgomery, D. R. (1997). A systematic analysis of eight  
784 decades of incipient motion studies, with special reference to gravel-bedded rivers.  
785 *Water Resources Research*, 33(8):1993–2029.
- 786 Camenen, B., Herrero, A., Dramais, G., Thollet, F., Le Bescond, C., Perret, E., and  
787 Berni, C. (2015). Field experiment on the dynamics of fine and coarse sediments  
788 over a gravel bar in an alpine river. In *Proc. 36th IAHR Congress*, The Hague,  
789 The Netherlands.
- 790 Camenen, B. and Larson, M. (2005). A general formula for non-cohesive bed load  
791 transport. *Estuarine, Coastal and Shelf Science*, 63:246–260.
- 792 Camenen, B., Le Coz, J., Paquier, A., and Lagouy, M. (2010). An estimation  
793 of gravel mobility over an alpine river gravel bar (Arc en Maurienne, France)  
794 using PIT-tag tracers. In Dittrich, A., Koll, K., Aberle, J., and Geisenhainer,  
795 P., editors, *River Flow, Proc. 5th International Conference on Fluvial Hydraulics*,  
796 pages 953–960, Braunschweig, Germany.
- 797 Chiew, Y.-M. and Parker, G. (1994). Incipient sediment motion on non-horizontal  
798 slopes. *Journal of Hydraulic Research*, 32:649–660.
- 799 Church, M., Hassan, M. A., and Wolcott, J. F. (1998). Stabilizing self-organized  
800 structures in gravel-bed stream channels: Field and experimental observations.  
801 *Water Resources Research*, 34(11):3169–3179.
- 802 Cooper, J. R. and Tait, S. J. (2009). Water-worked gravel beds in laboratory flumes  
803 - a natural analogue ? *Earth Surface Processes and Landforms*, 34(3):384–397.
- 804 Cui, Y., Wooster, J. K., Baker, P. F., Dusterhoff, S. R., Sklar, L. S., and Dietrich,  
805 W. E. (2008). Theory of fine sediment infiltration into immobile gravel bed.  
806 *Journal of Hydraulic Engineering*, 134(10):1421–1429.
- 807 Curran, J. and Wilcock, P. R. (2005). Effect of sand supply on transport rates in a  
808 gravel-bed channel. *Journal of Hydraulic Engineering*, 131(11).

- 809 Curran, J. C. (2007). The decrease in shear stress and increase in transport rates  
810 subsequent to an increase in sand supply to a gravel-bed channel. *Sedimentary*  
811 *Geology*, 202(3):572–580. Special issue: From Particle Size to Sediment Dynamics.
- 812 Curran, J. C. (2010). An investigation of bed armoring process and the formation  
813 of microclusters. In *2nd Joint Federal Interagency Conference*, Las Vegas, NV.
- 814 Durafour, M., Jarno, A., Le Bot, S., Lafite, R., and Marin, F. (2015). Bedload trans-  
815 port for heterogeneous sediments. *Environmental Fluid Mechanics*, 15(4):731–751.
- 816 Einstein, H. A. (1968). Deposition of suspended particles in a gravel bed. *Journal*  
817 *of Hydraulic Division*, 94(5):1197–1204.
- 818 Friedrich, H. (2010). Evaluation of statistical analysis techniques for developing  
819 bedforms recorded in 3d. Master’s thesis, The Departement of Civil and Environ-  
820 mental Engineering, the University of Auckland., New Zealand.
- 821 Frostick, L. E., Lukas, P. M., and Reid, I. (1984). The infiltration of fine matri-  
822 ces into coarse-grained alluvial sediments and its implications for stratigraphical  
823 interpretation. *Journal of the Geological Society*, 141:955–965.
- 824 Gibson, S., Abraham, D., Heath, R., and Schoellhamer, D. (2009). Vertical grada-  
825 tional variability of fines deposited in a gravel framework. *Sedimentology*, 56:661–  
826 676.
- 827 Gibson, S., Abraham, D., Ronald, H., and Schoellhamer, D. (2010). Bridging process  
828 threshold for sediment infiltrating into a coarse substrate. *Journal of Geotechnical*  
829 *and Geoenvironmental Engineering*, 136(2).
- 830 Guney, M. S., G., B., and Aksoy, A. (2013). Experimental study of the coarse  
831 surface development effect on the bimodal bed-load transport under unsteady  
832 flow conditions. *Journal of Hydraulic Engineering*, 139(1).
- 833 Hamm, N. T., Dade, W. B., and Renshaw, C. E. (2011). Fine particle deposition to  
834 porous beds. *Water Resources Research*, 47(W11508):1–13.

- 835 Hassan, M. A. and Church, M. (2000). Experiments on surface structure and partial  
836 sediment transport on a gravel bed. *Water Resources Research*, 36(7):1885–1895.
- 837 Hassan, M. A., Egozi, R., and Parker, G. (2006). Experiments on the effect of  
838 hydrograph characteristics on vertical grain sorting in gravel bed rivers. *Water*  
839 *Resources Research*, 42(9).
- 840 Haynes, H., Vignaga, E., and Holmes, W. M. (2009). Using magnetic resonance  
841 imaging for experimental analysis of fine-sediment infiltration into gravel beds.  
842 *Sedimentology*, 56(7):1961–1975.
- 843 Herrero, A. and Berni, C. (2016). Sand infiltration into a gravel bed: A mathematical  
844 model. *Water Resources Research*, 52(11):8956–8969.
- 845 Hill, K., Gaffney, J., Baumgardner, S., Wilcock, P., and Paola, C. (2017). Exper-  
846 imental study of the effect of grain sizes in bimodal mixture on bed slope, bed  
847 texture, and the transition to washload. *Water Resources Research*, 53:923–941.
- 848 Hodge, R., Sear, D., and Leyland, J. (2013). Spatial variations in surface sedi-  
849 ment structure in riffle-pool sequences: a preliminary test of the Differential Sedi-  
850 ment Entrainment Hypothesis (DSEH). *Earth Surface Processes and Landforms*,  
851 38:449–465.
- 852 Ikeda, H. and Iseya, F. (1988). Experimental study of heterogeneous sediment  
853 transport. Technical Report 12, Environmental Reserch Center, University of  
854 Tsukuba. 50p.
- 855 Jackson, W. L. and Beschta, R. L. (1984). Influences of increased sand delivery on  
856 the morphology of sand and gravel channel. *Journal - American Water Works*  
857 *Association*, 20(4):527–533.
- 858 Jain, R. K. and Kothyari, U. C. (2009). Cohesion influences on erosion and bed load  
859 transport. *Water Resources Research*, 45.

- 860 Koll, K. and Dittrich, A. (2010). Sediment transport over a static armour layer and  
861 its impact on bed stability. In Dittrich, A., Koll, K., Aberle, J., and Geisenhainer,  
862 P., editors, *River Flow, Proc. 5th International Conference on Fluvial Hydraulics*,  
863 pages 929–936, Braunschweig, Germany.
- 864 Kondolf, G. M. and Wolman, M. G. (1993). The sizes of salmonid spawning gravel.  
865 *Water Resources Research*, 29:2275–2285.
- 866 Kothyari, U. C. and Jain, R. K. (2008). Influence of cohesion on the incipient motion  
867 condition of sediment mixtures. *Water Resources Research*, 44(W04410).
- 868 Krishnappan, B. G. and Engel, P. (2006). Entrapment of fines in coarse sediment  
869 beds. In *River Flow, Proc. 3rd International Conference on Fluvial Hydraulics*,  
870 Lisbon, Portugal. Taylor & Francis.
- 871 Lamb, M. P., Dietrich, W. E., and Venditti, J. G. (2008). Is the critical shields  
872 stress for incipient sediment motion dependent on channel-bed slope? *Journal of*  
873 *Geophysical Research*, 113(F02008):20 p.
- 874 Leonardson, R. (2010). *Exchange of fine sediments with gravel riverbeds*. Phd thesis,  
875 Berkeley University, Berkeley, California, USA.
- 876 Li, Z. and Komar, P. D. (1986). Laboratory measurements of pivoting angle for appli-  
877 cations to selective entrainment of gravel in a current. *Sedimentology*, 33(3):413–  
878 423.
- 879 Lisle, T. E. (1989). Sediment transport and resulting deposition in spawning gravels,  
880 North Coastal California. *Water Resources Research*, 25(6):1303–1319.
- 881 Manes, C., Pokrajac, D., McEwan, I., and Nikora, V. (2009). Turbulence structure of  
882 open channel flows over permeable and impermeable beds: A comparative study.  
883 *Physics of Fluids*, 21(12):125109.
- 884 Mao, L. (2012). The effect of hydrographs on bed load transport and bed sediment  
885 spatial arrangement. *Journal of Geophysical Research: Earth Surface*, 117(F3).

- 886 Mao, L., Cooper, J. R., and Frostick, L. E. (2011). Grain size and topographic  
887 differences between static and mobile armour layers. *Earth Surface Processes and*  
888 *Landforms*, 36:1321–1334.
- 889 Marion, A., Tait, S. J., and McEwan, I. K. (2003). Analysis of small-scale gravel  
890 bed topography during armoring. *Water Resources Research*, 39(12-1334):1–11.
- 891 Marquis, G. A. and Roy, A. G. (2012). Using multiple bed load measurements:  
892 toward the identification of the bed dilation and contraction in gravel-bed rivers.  
893 *Journal of Geophysical Research*, 117(F01014):1–16.
- 894 Meyer-Peter, E. and Müller, R. (1948). Formulas for bed-load transport. In *Proc.*  
895 *2nd IAHR Congress*, pages 39–64, Stockholm, Sweden.
- 896 Mueller, E. R., Pitlick, J., and Nelson, J. M. (2005). Variation in the reference shields  
897 stress for bed load transport in gravel-bed streams and rivers. *Water Resources*  
898 *Research*, 41(W04006):1–10.
- 899 NF P 94-072 (1995). Sols: reconnaissance et essais. essai scissométrique en labora-  
900 toire. Technical report, AFNOR Norm.
- 901 Nikora, V. I., Goring, D. G., and Biggs, B. J. F. (1998). On gravel-bed roughness  
902 characterization. *Water Resources Research*, 34(3):517–527.
- 903 Nuñez Gonzalez, F. (2016). Infiltration of fine sediment mixtures through poorly  
904 sorted immobile coarse beds. *Water Resources Research*, 52(12):9306–9324.
- 905 Parker, G. (2008). *Sediment Engineering - Processes, Measurements, Modeling,*  
906 *and Practice (Editor: M.H. Garcia)*, chapter Transport of gravel and sediment  
907 mixtures, pages 165–252. American Society of Civil Engineers.
- 908 Parker, G., Klingeman, P. C., and McLean, D. G. (1982). Bed load and size distribu-  
909 tion in paved gravel-bed streams. *Journal of Hydraulics Division*, 108(HY4):544–  
910 571.

- 911 Perret, E., Berni, C., Herrero, A., Camenen, B., Buffet, A., and El kadi Abder-  
912 rezzak, K. (2016). Laser scanning method to characterize bed arrangement and  
913 its influence on incipient motion of gravel sediments. In *River Flow, Proc. 8th*  
914 *International Conference on Fluvial Hydraulics*, St Louis, USA.
- 915 Petit, F., Houbrechts, G., Peeters, A., Hallot, E., Van Campenhout, J., and Denis,  
916 A.-C. (2015). Dimensionless critical shear stress in gravel-bed rivers. *Geomor-*  
917 *phology*, 250:308–320.
- 918 Pitlick, J. and Van Steeter, M. M. (1998). Geomorphology and endangered fish  
919 habitats of the upper colorado river: 2. linking sediment transport to habitat  
920 maintenance. *Water Resources Research*, 34(2):303–316.
- 921 Proffitt, G. and Sutherland, A. (1983). Transport of non-uniform sediments. *Journal*  
922 *of Hydraulic Research*, 21(1):33–43.
- 923 Qin, J., Zhong, D., Wang, G., and Ng, S. L. (2012). On characterization of the  
924 imbrication of armored gravel surfaces. *Geomorphology*, 159-160:116–124.
- 925 Recking, A. (2009). Theoretical development on the effects of changing flow hy-  
926 draulics on incipient bedload motion. *Water Resources Research*, 45:1–16.
- 927 Recking, A., Libault, F., Peteuil, C., and Jolimet, T. (2012). Testing bedload  
928 transport equations with consideration of time scales. *Earth Surface Processes*  
929 *and Landforms*, 37(7):774–789.
- 930 Recking, A., Liébault, F., Peteuil, C., and Jolimet, T. (2012). Testing bedload  
931 transport equations with consideration of time scales. *Earth Surface Processes*  
932 *and Landforms*, 37:774–789.
- 933 Reid, I., Frostick, L. E., and Layman, J. T. (1985). The incidence and nature of  
934 bedload transport during flood flows in coarse-grained alluvial channels. *Earth*  
935 *Surface Processes and Landforms*, 10:33–44.

- 936 Sakthivadivel, R. and Einstein, H. A. (1970). Clogging of porous column of spheres  
937 by sediment. *Journal of the Hydraulics Division*, 96(2):461–472.
- 938 Schälchli, U. (1992). The clogging of coarse gravel river beds by fine sediment.  
939 *Hydrobiologia*, 235-236(1):189–197.
- 940 Sear, D. A. (1993). Fine sediment infiltration into gravel spawning beds within a reg-  
941 ulated river experiencing floods: ecological implications for salmonids. *Regulated*  
942 *Rivers: Research and Management*, 8:373–390.
- 943 Shields, A. (1936). Anwendung der Ähnlichkeits-mechanik und der turbulenz-  
944 forschung auf die geschlebebewegung. *Preussische Versuchsanstalt für Wasserbau*  
945 *und Schiffbau*, 26:26 p. Berlin, Germany.
- 946 Shvidchenko, A. B. and Pender, G. (2000). Flume study of the effect of relative  
947 depth on the incipient motion of coarse uniform sediments. *Water Resources*  
948 *Research*, 36(2):619–628.
- 949 Smart, G. M., Maurice, M. J., and Walsh, J. M. (2002). Relatively rough flow  
950 resistance equations. *Journal of Hydraulic Engineering*, 128(6):568–578.
- 951 Soulsby, R. L. (1997). *Dynamics of marine sands, a manual for practical applica-*  
952 *tions*. Thomas Telford, London, UK. ISBN 0-7277-2584 X.
- 953 Soulsby, R. L. and Whitehouse, R. J. S. W. (1997). Threshold of sediment motion in  
954 coastal environment. In *Proc. Pacific Coasts and Ports'97 Conf.*, pages 149–154,  
955 Christchurch, New Zealand. University of Canterbury.
- 956 Tait, S. (1993). *The physical processes of bed armouring in mixed grain sediment*  
957 *transport*. PhD thesis.
- 958 USWES (1935). Studies of river bed materials and their movement with special  
959 reference to the lower Mississippi River. Technical Report 17, U. S. Army Corps  
960 of Engineers, Vicksburg, Mississippi, U. S. A. 161 pp.

- 961 Vanoni, V. A. and Brooks, N. H. (1957). Laboratory studies of the roughness  
962 and suspended load of alluvial streams. Technical report, Sedimentation Lab. ,  
963 California Institute of Technology, Pasadena, California, USA.
- 964 Voepel, H., Ahmed, S., Hodge, R., Leyland, J., and Sear, D. (2017). Variations  
965 in grain-scale sediment structure and entrainment force in a gravel-bed channel  
966 as a function of fine sediment content and morphological location. In *European*  
967 *Geophysical Union*, Vienna.
- 968 Wainwright, J., Parsons, A. J., Cooper, J. R., Gao, P., Gillies, J. A., Mao, L.,  
969 Orford, J. D., and Knight, P. G. (2015). The concept of transport capacity in  
970 geomorphology. *Reviews of Geophysics*, 53.
- 971 Wharton, G., Mohajeri, S., and Righetti, M. (2017). The pernicious problem of  
972 streambed colmatation: a multi-disciplinarity reflection on the mechanisms, causes,  
973 impacts, and management challenges. *Wiley Interdisciplinary Reviews: Water*,  
974 4:1–17.
- 975 Wilcock, P., Potlick, J., and Cui, Y. (2009). Sediment transport primer: estimating  
976 bed-material transport in gravel-bed rivers. Technical report, U. S. Department  
977 of Agriculture, Forest Service, Rocky Mountain Research Station.
- 978 Wilcock, P. R. (2001). Toward a practical method for estimating sediment transport  
979 rates in gravel-bed rivers. *Earth Surface Processes and Landforms*, 26:1395–1408.
- 980 Wilcock, P. R. and Crowe, J. C. (2003). Surface-based transport model for mixed-  
981 size sediment. *Journal of Hydraulic Engineering*, 129(2):120–128.
- 982 Wilcock, P. R. and Kenworthy, S. T. (2002). A two-fraction model for the transport  
983 of sand/gravel mixtures. *Water Resources Research*, 38(10):1194.
- 984 Wilcock, P. R., Kenworthy, S. T., and Crowe, J. C. (2001). Experimental study of  
985 the transport of mixed sand and gravel. *Water Resources Research*, 37:3349–3358.

- 986 Wilcock, P. R. and McArdell, B. W. (1993). Surface-based fractional transport rates:  
987 Mobilization thresholds and partial transport of a sand-gravel sediment. *Water*  
988 *Resources Research*, 29(4):1297–1312.
- 989 Wren, D. G., Langendoen, E. J., and Kuhnle, R. A. (2011). Effects of sand addition  
990 on turbulent flow over an immobile gravel bed. *Journal of Geophysical Research:*  
991 *Earth Surface*, 116(F1).
- 992 XP CEN ISO/TS 17892-6 (2006). Reconnaissance et essais géotechniques - essais de  
993 laboratoire sur les sols - partie 6 : essai de pénétration de cône. Technical report,  
994 AFNOR norms.
- 995 Yalin, M. and Karahan, E. (1979). Inception of sediment transport. *Journal of*  
996 *Hydraulic Engineering*, 105:1433–1443.

Table 1: Main geometrical and geotechnical characteristics of the sediments or mixtures used in this study.

Sediments	$D_{50}, d_{50}$ (mm)	$\sigma_g$ (-)	$w_s$ (mm/s)	$CI$ (-)	$p$ (-)	$k$ (m <sup>2</sup> )	$C_{u-sat}$ (kPa)	$C_{u-20-30\%}$ (kPa)	$Re_k$ (-)
G	6.8	1.3	340	0.84	0.42	$3.6 \cdot 10^{-8}$	0	0	15.7
S	0.813	1.34	110	0.84	NE	NE	0	0	NE
FS	0.066	1.3	3.6	0.99	0.4	$3.4 \cdot 10^{-12}$	0	11-12	0.15
MS	0.04	2.5	1.3	0.75	0.56	$3.4 \cdot 10^{-12}$	2.4-28	250-500	0.15
Mixtures									
G/FS	NE	NE	NA	NA	0.17	$1.9 \cdot 10^{-11}$	NE	NE	0.36
G/Ms	NE	NE	NA	NA	0.23	$6.7 \cdot 10^{-11}$	NE	NE	0.68

$D_{50}$  and  $d_{50}$  are the median grain diameters of the coarse and fine sediments, respectively [mm];  $\sigma_g$  is the geometric standard deviation of the GSD;  $w_s$  is the settling velocity computed using Soulsby (1997) equation;  $CI$  is the circularity index;  $p$  is the bed porosity; Mixture porosity were calculated using the comparison between gravel porosity and the maximum fine content that can contain the gravel matrix as presented in Leonardson (2010).  $k$  is the bed permeability computed with the Kozeny-Carman relation;  $C_{u-sat}$  is the bed consolidation measured for water-saturated beds;  $C_{u-20-30\%}$  is the bed consolidation measured when the bed water content is about 20-30%;  $Re_k = \sqrt{k}u^*/\nu$  is the permeability Reynold number;  $u^* = \sqrt{ghI}$  is calculated for a standard case where  $I = 0.01$  and  $h = 0.07$  m. NE and NA refer to not evaluated and not applicable data, respectively.